Neuron

Article

Nav1.7 is essential for nociceptor action potentials in the mouse in a manner independent of endogenous opioids

Graphical abstract

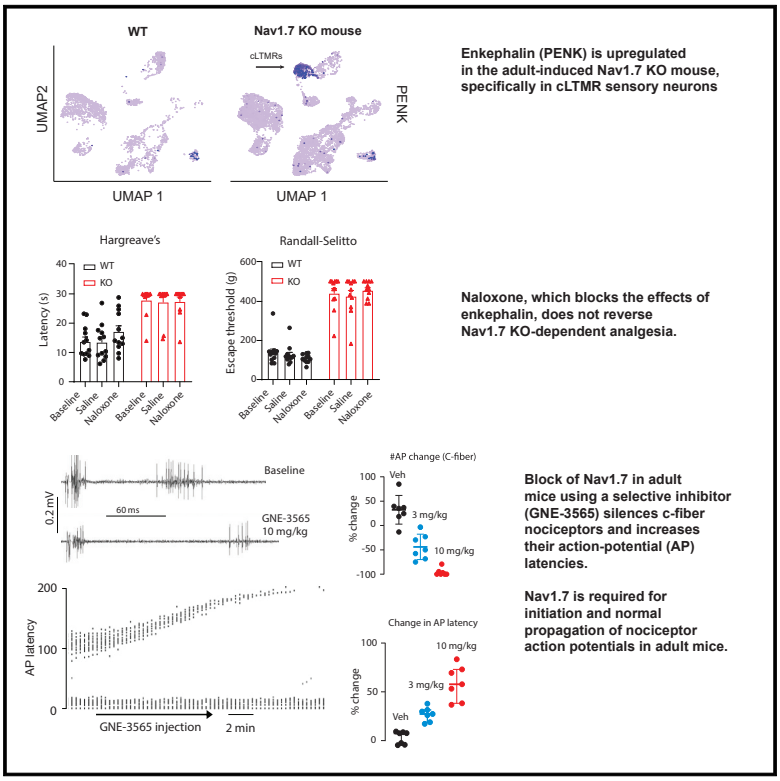

Highlights

- *Penk* (pro-enkephalin) is upregulated following induced removal of Nav1.7 in adult mice
- *Penk* upregulation in the DRG is specific for cLTMRs
- Analgesia observed after Nav1.7 removal is not driven by enkephalin overexpression
- Nav1.7 plays an essential role in the initiation of nociceptor action potentials

Authors

Lunbin Deng, Michelle Dourado, Rebecca M. Reese, ..., Paul Karila, Julien Allard, David H. Hackos

Correspondence

julien.allard@e-phys.com (J.A.), hackos.david@gene.com (D.H.H.)

In brief

Deng et al. show that genetic removal or selective inhibition of Nav1.7 blocks nociceptor action potentials, highlighting the essential role Nav1.7 plays in initiating such APs and explaining the resulting analgesia. Enkephalin overexpression, previously thought to drive analgesia in Nav1.7 knockout mice, was found to play a limited role, if any.

Deng et al., 2023, Neuron *111*, 1–18
September 6, 2023
https://doi.org/10.1016/j.neuron.2023.05.024

CellPress

Neuron

CellPress
OPEN ACCESS

Article

Nav1.7 is essential for nociceptor action potentials in the mouse in a manner independent of endogenous opioids

Lunbin Deng,[1] Michelle Dourado,[1] Rebecca M. Reese,[1] Kevin Huang,[2] Shannon D. Shields,[1] Kimberly L. Stark,[1] James Maksymetz,[1] Han Lin,[1] Joshua S. Kaminker,[2] Min Jung,[2] Oded Foreman,[3] Janet Tao,[3] Hai Ngu,[3] Victory Joseph,[4] Meron Roose-Girma,[5] Lucinda Tam,[5] Susanne Lardell,[6] Linnea Strid Orrhult,[6] Paul Karila,[6] Julien Allard,[7,*] and David H. Hackos[1,8,*]

[1]Department of Neuroscience, Genentech, Inc., 1 DNA Way, South San Francisco, CA, USA
[2]Department of OMNI Bioinformatics, Genentech, Inc., 1 DNA Way, South San Francisco, CA, USA
[3]Department of Pathology, Genentech, Inc., 1 DNA Way, South San Francisco, CA, USA
[4]Department of Biomedical Imaging, Genentech, Inc., 1 DNA Way, South San Francisco, CA, USA
[5]Department of Molecular Biology, Genentech, Inc., 1 DNA Way, South San Francisco, CA 94080, USA
[6]Cellectricon AB, Neongatan 4B, 431 53 Mölndal, Sweden
[7]E-Phys, CRBC, 28 place Henri Dunant, 63000 Clermont-Ferrand, France
[8]Lead contact
*Correspondence: julien.allard@e-phys.com (J.A.), hackos.david@gene.com (D.H.H.)
https://doi.org/10.1016/j.neuron.2023.05.024

SUMMARY

Loss-of-function mutations in Nav1.7, a voltage-gated sodium channel, cause congenital insensitivity to pain (CIP) in humans, demonstrating that Nav1.7 is essential for the perception of pain. However, the mechanism by which loss of Nav1.7 results in insensitivity to pain is not entirely clear. It has been suggested that loss of Nav1.7 induces overexpression of enkephalin, an endogenous opioid receptor agonist, leading to opioid-dependent analgesia. Using behavioral pharmacology and single-cell RNA-seq analysis, we find that overexpression of enkephalin occurs only in cLTMR neurons, a subclass of sensory neurons involved in low-threshold touch detection, and that this overexpression does not play a role in the analgesia observed following genetic removal of Nav1.7. Furthermore, we demonstrate using laser speckle contrast imaging (LSCI) and *in vivo* electrophysiology that Nav1.7 function is required for the initiation of C-fiber action potentials (APs), which explains the observed insensitivity to pain following genetic removal or inhibition of Nav1.7.

INTRODUCTION

Genetic evidence demonstrates that the voltage-gated sodium channel Nav1.7 is essential for pain in humans. In particular, people who lack a functional copy of the gene that encodes Nav1.7, *Scn9a*, have congenital insensitivity to pain (CIP) and are completely unable to experience any form of pain or nociception,[1,2] whereas gain-of-function mutations lead to painful neuropathies such as inherited erythromelalgia (IEM),[3–6] paroxysmal extreme pain disorder (PEPD),[7–9] and small fiber neuropathies.[10] Given that voltage-gated sodium channels are in principle druggable targets, Nav1.7 has been considered an important target for novel non-opioid pain drugs.[11]

Voltage-gated sodium (Nav) channels play an essential role in the generation of action potentials (APs) in neurons and other electrically excitable cells.[12,13] Each Nav channel is made up of a single alpha subunit and zero, one, or two beta subunits. In mammals, there are nine separate Nav alpha subunits (Nav1.1–1.9), each with distinct biophysical properties and tissue expression patterns. Adult nociceptor neurons, the sensory neurons responsible for detecting noxious signals, primarily express Nav1.7, Nav1.8, and Nav1.9, with lower levels of Nav1.1 and Nav1.6.[14,15] While it is clear that peripheral Nav channel function is required for the initiation and propagation of APs in nociceptors, the precise role that each of the five Nav channels present in nociceptors play in this process is not fully understood.

Two of the nociceptor Nav channels, Nav1.8 and Nav1.9, can be pharmacologically distinguished from the others since the pufferfish toxin tetrodotoxin (TTX) blocks these channels with >1,000-fold reduced potency relative to TTX-sensitive (TTX-S) Nav channels such as Nav1.1, Nav1.6, and Nav1.7. It is known that in nociceptors, sequential activation of TTX-S channels followed by Nav1.8 occurs during the AP.[16,17] However, since TTX exerts powerful local anesthetic effects, it is clear that block of TTX-S Nav channels alone is sufficient to prevent initiation and/or propagation of APs in nociceptors.[18–21] Given that Nav1.7 is the major nociceptor TTX-S Nav channel, it is reasonable to expect that genetic loss of function of Nav1.7 results in

Please cite this article in press as: Deng et al., Nav1.7 is essential for nociceptor action potentials in the mouse in a manner independent of endogenous opioids, Neuron (2023), https://doi.org/10.1016/j.neuron.2023.05.024

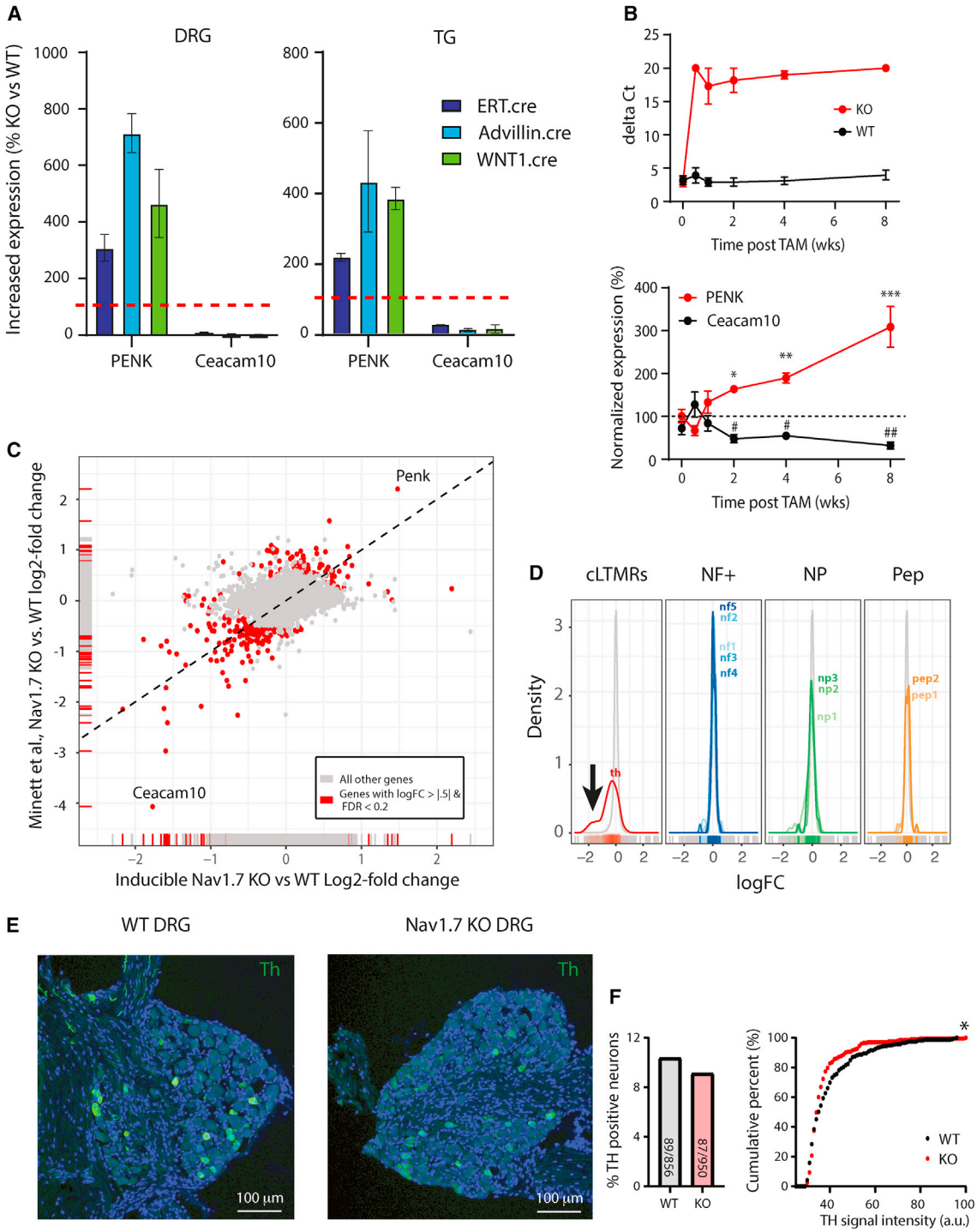

Figure 1. Gene expression changes in the DRG following genetic removal of Nav1.7

(A) Increased expression of *Penk* and decreased expression of *Ceacam10* in DRGs or TGs obtained from three different Nav1.7 KO mice (ERT.cre, Advillin.cre, and WNT1.cre). Dashed red line indicates average expression level observed in cre.neg mice from all three colonies (n = 3 mice per group).

(B) Time course of gene expression changes in DRGs obtained from ERT.cre Nav1.7 KO mice following tamoxifen (TAM) injection. Top panel shows rapid loss of Nav1.7 transcripts in KO mice (red) vs. cre.neg controls (black) (log_2 scale). Lower panel shows the time dependence of increasing *Penk* expression and decreasing *Ceacam10* expression (linear scale) (n = 3–9 mice per time point, one-way ANOVA, *p < 0.05, **p < 0.01, ***p < 0.001).

(legend continued on next page)

CIP because nociceptors are no longer able to initiate and/or propagate APs.

However, recently an alternative mechanism has been proposed that suggests that in the absence of Nav1.7, sensory neurons overexpress the endogenous opioid enkephalin via upregulation of the *Penk* gene.[22,23] This increased level of enkephalin would then bind to μ-opioid receptors in the spinal cord, resulting in a morphine-like loss of pain sensation. This hypothesis was tested by dosing Nav1.7 knockout (KO) mice (as well as a single CIP patient) with the opioid receptor blocker naloxone, which was reported to restore normal pain behavior in Nav1.7 KO mice.[23] In fact, it has recently been reported that nociceptor APs remain intact in the Nav1.7 KO mouse,[24] suggesting that Nav1.7 may not be required for nociceptor APs *in vivo* at all.

Understanding the mechanism by which block of Nav1.7 leads to analgesia is important for drug discovery efforts. In particular, the endogenous opioid mechanism might be undesirable and lead to opioid-like side effects such as tolerance and tachyphylaxis. In order to examine the role that the endogenous opioid mechanism plays from a therapeutic perspective, we chose to use an adult-inducible Nav1.7 KO mouse that better models therapeutic block of Nav1.7 and avoids potential effects of removal of Nav1.7 during early development. We found that following tamoxifen (TAM)-induced deletion of Nav1.7, *Penk* was upregulated in the dorsal root ganglion (DRG), as has been previously reported in mice with early-developmental deletion of Nav1.7. However, block of μ-opioid receptors by dosing mice with naloxone did not alter the CIP-like phenotype of adult-inducible Nav1.7 KO mice, suggesting that *Penk* overexpression is not responsible for the analgesic phenotype. Further support for the non-essential role of *Penk* was obtained by demonstrating that a selective inhibitor of Nav1.7 is able to replicate the CIP-like phenotype in mice within 1 h after dosing, prior to changes in *Penk* expression. Additionally, we noticed that *Penk* upregulation is restricted specifically to cLTMRs (c-type low threshold mechano-receptors), a population of non-myelinated DRG neurons that do not function as nociceptors. We then constructed a conditional KO mouse where Nav1.7 is selectively removed from cLTMRs and showed that *Penk* upregulation occurs to the same extent and in the same DRG cell types (cLTMRs) as in the full-body inducible KO mouse. Behavioral analysis of this conditional KO mouse, where Nav1.7 is expressed at normal levels in nociceptors, shows normal pain behavior, strongly suggesting that *Penk* upregulation in cLTMRs plays no role in the CIP-like phenotype of adult-inducible Nav1.7 KO mice.

On the other hand, laser contrast speckle imaging (LCSI) experiments used to detect action-potential-mediated increases in blood flow following allyl isothiocyanate (AITC) treatment of the hind paw suggest that APs fail to initiate in the periphery following the genetic removal of Nav1.7 or block with a selective inhibitor. In addition, *in vivo* recordings of sensory neuron APs recorded either indirectly from wide dynamic range (WDR) neurons in the dorsal horn of the spinal cord or directly from DRG neurons reveal that selective Nav1.7 inhibition is able to silence C-fibers and increase AP latency while having no effect on A-fibers, directly demonstrating that C-fiber APs depend on Nav1.7.

RESULTS

Increased DRG enkephalin expression and decreased expression of cLTMR-specific genes occurs after genetic removal of Nav1.7

It has been reported that *Penk* (pro-enkephalin) is upregulated in DRG neurons in Nav1.7 KO mice, leading to increased enkephalin levels in the dorsal spinal cord and μ-opioid-receptor-dependent analgesia.[23] To examine this further, we started by determining the expression of *Penk* and *Ceacam10* in two conditional Nav1.7 loss-of-function mouse models (Nav1.7 fl/fl;WNT1.cre, Nav1.7 fl/fl;Advillin.cre) as well as a TAM-inducible Nav1.7 KO mouse (Nav1.7 fl/fl;ERT.cre) 8 weeks following TAM injection. In all three cases, we observed marked increases in *Penk* expression and decreases in *Ceacam10* expression in both the DRG and the trigeminal ganglion (TG) (Figure 1A). Since Nav1.7 is a very stable protein, decreases in Nav1.7 protein expression significantly lags rapid removal of Nav1.7 mRNA following TAM dosing (Tau = 1.1 weeks).[25] We examined the time course of mRNA levels of *Penk* and *Ceacam10* for 8 weeks following TAM injection and observed slow increases in *Penk* expression and slow decreases in *Ceacam10* expression with similar time courses relative to falling Nav1.7 protein levels (Figure 1B). We next performed bulk RNA sequencing (RNA-seq) analysis from DRGs collected at the 8-week time point. We compared gene expression changes in TAM-induced Nav1.7 KO mice vs. TAM-injected WT littermate control mice to the expression changes observed in Minett et al.[23] and found a similar set of differentially expressed genes (Figure 1C). In fact, *Penk* is one of the genes showing the highest level of increased expression in both datasets. We noticed that some of the genes showing decreased levels of expression, such as *Ceacam10*, are known to be selectively expressed in cLTMR neurons,[26] a subclass of non-myelinated DRG neurons proposed to play a role in "pleasant touch." To examine this further, we performed histogram analysis using sets of genes known to be selectively expressed in different subclasses of DRG neurons and found that only cLTMRs showed decreases in expression of DRG subclass-specific genes (Figure 1D). Similar cLTMR-specific gene expression changes were observed in the data from Minett et al.[23] (Figure S1). No DRG-subtype-specific changes were observed in Nav1.8 KO mice or

(C) Results of bulk-seq RNA sequencing comparing our data from cre.neg (WT) vs. cre.pos (KO) ERT.cre; fl/fl Nav1.7 mice vs. similar published data from Minett et al.[23] Red points indicate genes showing $\log_2$ fold changes of >|0.5| and a false discovery rate (FDR) < 0.2. *Penk* and *Ceacam10* (labeled) show large changes in expression in both datasets.

(D) Histogram analysis showing $\log_2$ fold changes of genes selectively expressed in specific sets of DRG neurons (see STAR Methods). The gray histograms represent all genes for comparison. Arrow indicates cLTMR-specific genes are down-regulated in the Nav1.7 KO mouse (n = 6 mice per genotype).

(E) Immunohistochemical (IHC) staining of tyrosine hydroxylase (TH) in DRGs obtained from cre.neg (WT) and cre.pos (Nav1.7 KO) ERT.cre; fl/fl Nav1.7 mice.

(F) Analysis of IHC staining showing the percentage of TH+ vs. TH-DRG neurons (left) and the TH signal intensity shown as a cumulative percentage of observed neurons (right). Significantly more KO neurons show lower TH staining intensity vs. WT neurons (Kolmogorov-Smirnov test, $p < 0.05$, n = 6 mice per genotype).

Please cite this article in press as: Deng et al., Nav1.7 is essential for nociceptor action potentials in the mouse in a manner independent of endogenous opioids, Neuron (2023), https://doi.org/10.1016/j.neuron.2023.05.024

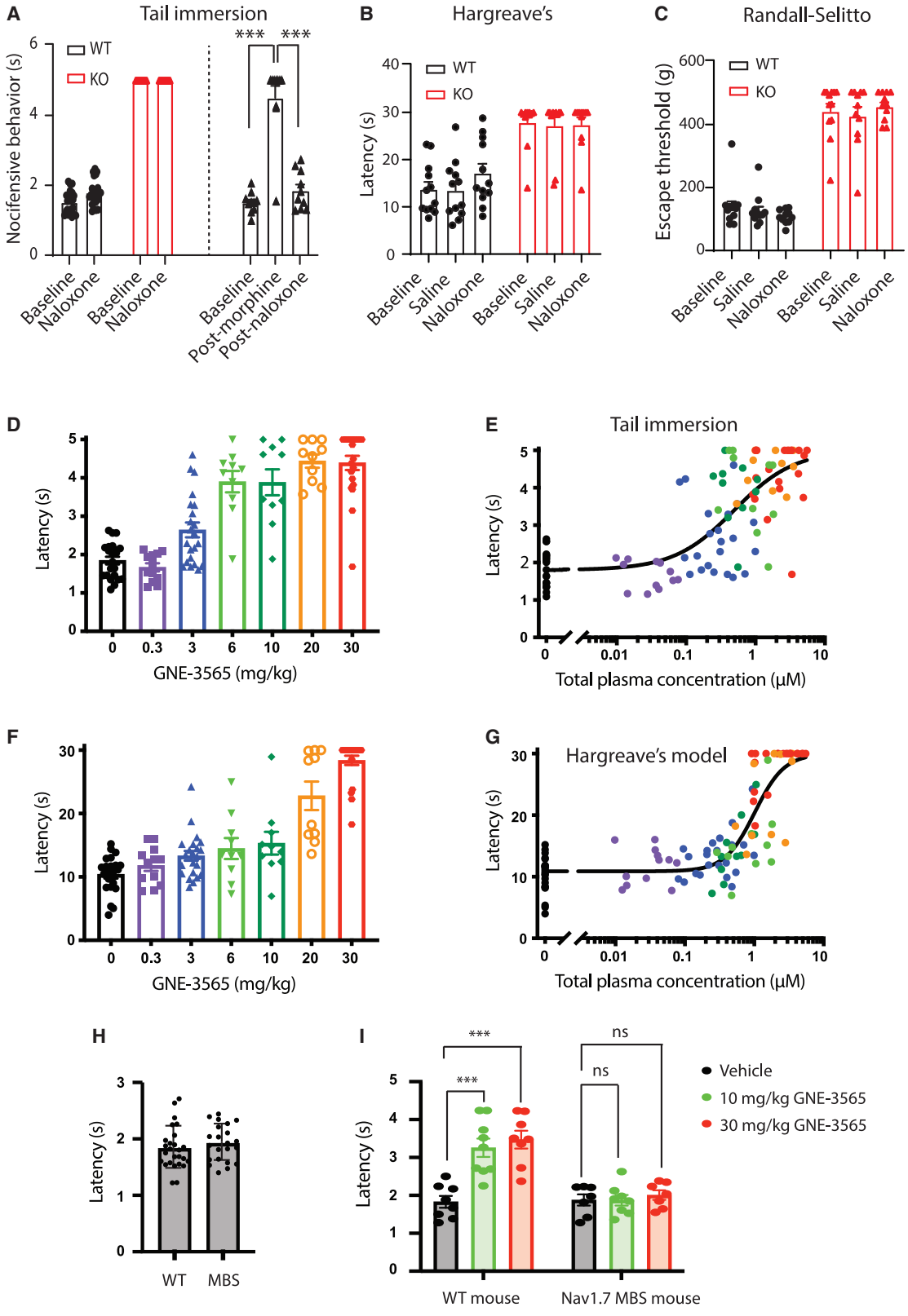

(legend on next page)

Nav1.9 KO mice (Figure S1), indicating that this effect is specific to Nav1.7 loss of function. We also found similar changes in *Penk* and *Ceacam10* expression in the superior cervical ganglion (SCG), which is part of the sympathetic nervous system and also expresses Nav1.7 (Figures S2A and S2B).

Decreases in expression of genes specific to cLTMRs could potentially be due to selective cell death of cLTMRs following Nav1.7 knockdown. To examine this possibility, we stained mouse DRG slices for cLTMRs using the specific marker tyrosine hydroxylase (*Th*) (Figure 1E). We observed that approximately 10% of DRG neurons were *Th*+, consistent with literature values of the percentage of DRG neurons that are cLTMRs.[27] Furthermore, we observed no significant differences in the percentage of *Th*+ DRG neurons between WT and Nav1.7 KO mice, though there was a significant decrease in the average brightness of *Th* staining in Nav1.7 KO DRGs (Figure 1F) as expected given the reduced expression of *Th* (like other cLTMR-specific genes). We also observed a small increase in enkephalin immunostaining within the dorsal horn of the spinal cord, as expected since enkephalin peptides are transported into the central termini of DRG neurons (Figures S2C and S2D).

Naloxone fails to reverse Nav1.7 knockdown-dependent analgesia in mice

TAM-induced removal of Nav1.7 expression using the Nav1.7 fl/fl; ERT.cre mouse results in profound analgesia in multiple models of nociception.[25] To determine if increased expression of *Penk* and subsequent increases in dorsal horn enkephalin peptide levels is responsible for this analgesia, we tested whether the μ-opioid inhibitor naloxone was able to reverse the Nav1.7 KO-dependent analgesia in three different nociception models (tail immersion, Hargreave's, and Randall-Selitto) (Figures 2A–2C). We observed no evidence of reversal of analgesia nor changes in baseline nociception of WT mice following i.v. injection of 100 ng naloxone. To make sure the naloxone was working properly, we demonstrated that morphine-dependent analgesia in the tail immersion model could be reversed following i.v. injection of 100 ng naloxone (Figure 2A).

Analgesia observed after oral dosing of a selective Nav1.7 inhibitor is too rapid to be explained by enkephalin expression

If *Penk* upregulation following genetic removal of Nav1.7 or pharmacological block of Nav1.7 is driving the observed analgesia, such analgesia would require time to develop as *Penk* needs to be expressed, processed into enkephalin peptide, transported to the central termini, and released into the dorsal horn of the spinal cord. Rapid block of Nav1.7 by a selective inhibitor should therefore show limited efficacy initially, with increasing efficacy building up over time as enkephalin levels in the spinal cord eventually increase. To test this idea, we chose the highly potent and selective Nav1.7 inhibitor, GNE-3565 (Figure S3A). This compound blocks Nav1.7 with sub-nM potency and is >1,000-fold selective over most Nav subtypes (Figures S3B and S3C). As with other aryl-sulfonamide Nav1.7 inhibitors, the exception is Nav1.2 and Nav1.6, where GNE-3565 shows partial selectivity of 19.7-fold and 22.5-fold, respectively. GNE-3565 achieves its high selectivity by interacting with the YW motif within the domain IV voltage-sensing domain (VSD4), where YW is present only in Nav1.2, Nav1.6, and Nav1.7, as well as the nearby valine residue V1541, which is leucine or methionine in other Nav channels.[28] Both mutations YW → SR and V1541L reduce the potency of GNE-3565, and the combination YWV → SRL reduces potency by >100-fold without altering the biophysical properties of Nav1.7 (Figures S3D and S3E). The zwitterionic character of GNE-3565 allows this compound to attain high free plasma concentrations (relatively low plasma protein binding) *in vivo* following either oral or i.v. dosing (Figure S3A). Furthermore, since GNE-3565 is a rapidly transported Pgp (P-glycoprotein) substrate, levels in the brain and spinal cord following dosing are expected to be too low to significantly engage the Nav1.7 target in the CNS.

We first tested GNE-3565 in a humanized mouse model of acute nociception. In this transgenic model, human Nav1.7 containing the single point mutation I848T that causes IEM in humans is expressed in DRG neurons alongside the native mouse Nav1.7. These mice show nocifensive responses to the plant alkaloid aconitine when injected into the dorsum of the hind paw that are dependent on functional human Nav1.7 channels.[29] We find that GNE-3565, dosed orally 1 h prior to testing, shows a dose-dependent decrease in nocifensive responses with an EC_{50} of 0.03 μM (Figures S3F and S3G). As this compound is 3.6% free in plasma, this EC_{50} represents a free plasma concentration of 1 nM, which is approximately equal to the *in vitro* IC50 of this compound. This indicates that blocking approximately 50% of Nav1.7 channels is required to show a 50% reduction in pain in this model.

We next tested GNE-3565 in two models of acute nociception following oral dosing (testing was performed 1 h post dosing, prior to any observed changes in *Penk* or *Ceacam10* expression;

Figure 2. Behavioral effects of naloxone on Nav1.7 KO mice and effects of GNE-3565

(A) Tail immersion experiment in cre.neg (WT, black) and cre.pos (Nav1.7 KO, red) ERT.cre; fl/fl Nav1.7 mice measured 6–8 weeks after tamoxifen dosing. Naloxone injection did not reverse the analgesia observed in Nav1.7 KO mice (n = 22 mice per group, two-way ANOVA, non-significant), while naloxone reversed morphine-induced analgesia in the same model (right, n = 10 mice per group, one-way ANOVA with Sidak's multiple comparisons test; $p < 0.001$ baseline vs. post-morphine; $p < 0.001$ post-morphine vs. post naloxone).

(B) Heat nociception (Hargreave's). Naloxone failed to reverse analgesia (n = 12 mice per group).

(C) Mechanical nociception (Randall-Sellito, tail). Naloxone failed to reverse analgesia (n = 12 mice per group, one-way ANOVA).

(D) GNE-3565 suppresses heat nociception (tail immersion model) in a dose-dependent manner (n = 10–30 per group).

(E) PK-PD (pharmicokinetic-pharmicodynamic) plot of GNE-3565 induced suppression of heat nociception (tail immersion) (n = 10–30 per group).

(F) GNE-3565 suppresses heat nociception (Hargreave's) in a dose-dependent manner (n = 10–30 per group).

(G) PK-PD plot of GNE-3565 induced suppression of heat nociception (Hargreave's) (n = 10–30 per group).

(H) Tail immersion latencies at baseline showing no difference between WT and Nav1.7 MBS mice (n = 23 per group).

(I) GNE-3565 suppresses heat nociception (tail immersion) in WT but not Nav1.7 MBS mice (n = 8 per group, two-way ANOVA, $p < 0.01$).

Please cite this article in press as: Deng et al., Nav1.7 is essential for nociceptor action potentials in the mouse in a manner independent of endogenous opioids, Neuron (2023), https://doi.org/10.1016/j.neuron.2023.05.024

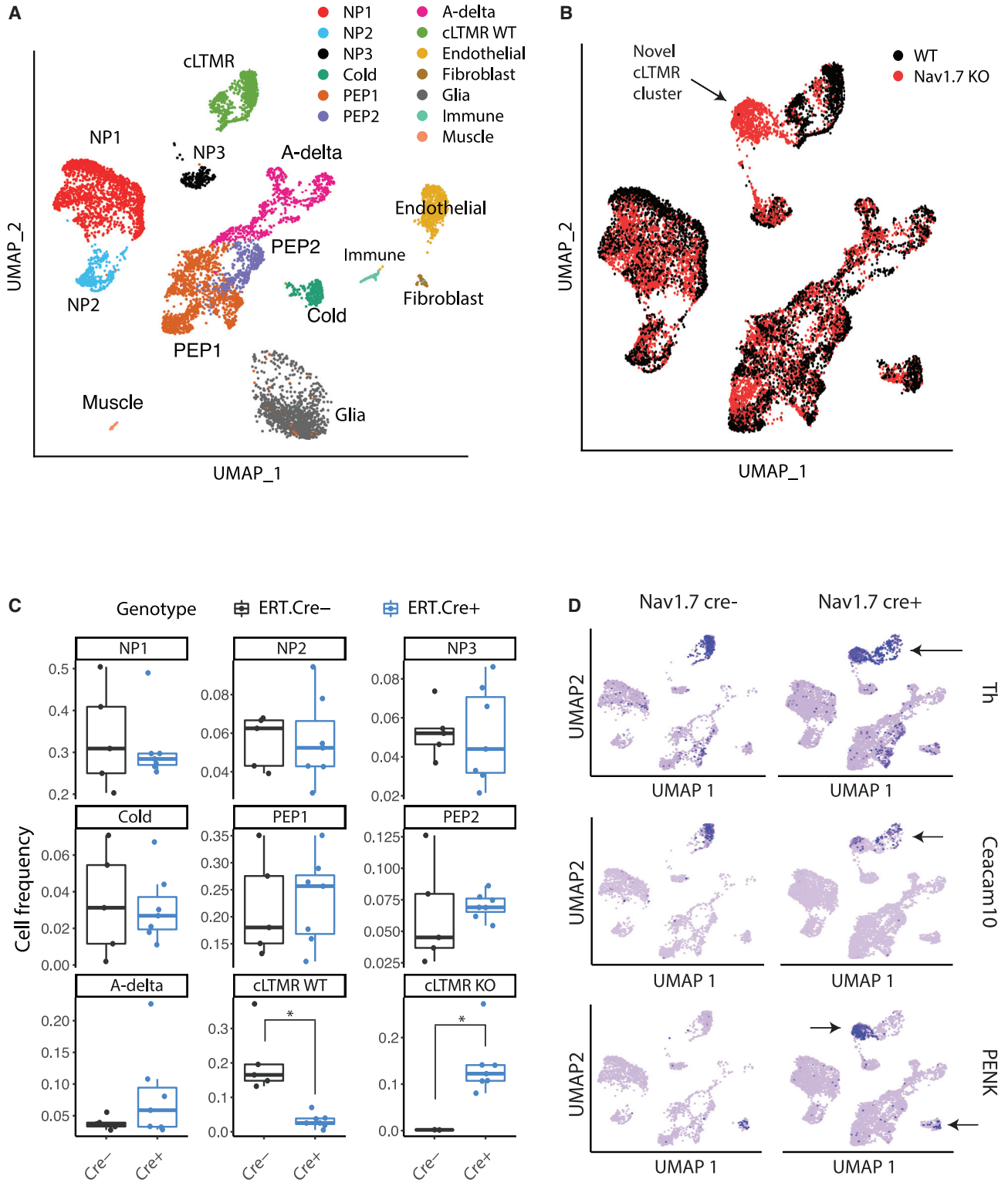

Figure 3. Single-cell RNA-seq analysis of WT and Nav1.7 KO DRG neurons

(A) UMAP showing the different populations of cells within the DRGs of WT mice (see STAR Methods).

(B) Neuronal UMAP overlay colored by genotype showing good overlap between WT and Nav1.7 KO clusters. An exception is the appearance of a new cluster adjacent to the cLTMR cluster that only appears in the Nav1.7 KO (indicated by arrow).

(legend continued on next page)

Figure S3H). GNE-3565 was able to fully inhibit the nociception reflex in the tail flick model at total plasma concentrations around 5 μM and an EC_{50} of 0.6 μM (Figures 2D and 2E) and was able to fully inhibit heat nociception (Hargreave's test) at total plasma concentrations around 5 μM and an EC_{50} of 1.0 μM (Figures 2F and 2G). These EC_{50} values are approximately 20-fold over the EC_{50} observed in the I848T transgenic model, which indicates that 50% reversal of acute heat nociception requires >90% inhibition of Nav1.7 channels. These high plasma concentrations likely have off-target effects that might contribute to the observed analgesic activity. In particular, while the mice show normal blood pressure (BP) (Figures S4A and S4B) and minimal impairment in an open-field test, some open-field impairment was observed at the highest dose tested (30 mg/kg) (Figures S4C and S4D). To demonstrate that the observed analgesic effects of GNE-3565 are strictly due to Nav1.7 inhibition, we constructed a mouse line (referred to as the Nav1.7 modified binding site [MBS] mouse) with the mutation at the aryl-sulfonamide-binding site (YWV → SRL) that decreases the affinity of GNE-3565 by >100-fold (Figure S3). As expected, DRG neurons from these mice show significantly reduced affinity for GNE-3565, demonstrating that the MBS mice express the mutant Nav1.7 channel (Figure S3I). We found that GNE-3565 failed to induce analgesia in Nav1.7 MBS mice (Figures 2H and 2I) while still showing impairment in the open-field test at 30 mg/kg (Figures S4E and S4F), demonstrating that the analgesic effects of GNE-3565 are specific to Nav1.7 inhibition and the open-field impairment is due to an off-target effect. These data therefore demonstrate that near-complete reversal of heat nociception (to levels similar to what is observed in Nav1.7 KO mice) can be rapidly achieved following dosing of a peripherally restricted selective Nav1.7 inhibitor.

Penk overexpression after genetic removal of Nav1.7 is specific to cLTMRs

We have found that following TAM-induced Nav1.7 knockout, *Penk* expression increases significantly in the DRG. We next attempted to determine in which DRG cell-type *Penk* increases are occurring. We thus performed single-cell RNA-seq (scRNA-seq) analysis on DRGs taken from either tamixofen-induced Nav1.7 KO mice (following 8 weeks post-TAM dosing) or cre.neg WT littermates (also dosed with TAM). DRG neurons were enzymatically dissociated, and single neurons were barcoded and sequenced using 10× Genomics technology. Analysis of these data allowed us to generate a UMAP (Uniform Manifold Approximation and Projection) showing the different cell-type clusters present in these samples (Figure 3A). We identified the different DRG neuron cell clusters by manual inspection of previously reported marker genes.[26] Interestingly, following Nav1.7 knockout, a distinct cell cluster appeared in the UMAP adjacent to the cLTMR cluster (Figure 3B). We noticed that the fraction of cells identified as cLTMRs significantly decreased ($p = 0.002$, Student's t test) while the fraction of cells corresponding to the novel cluster significantly increased ($p = 0.001$, Student's t test) (Figure 3C). Other DRG neuron cell types did not show significant changes in cell frequency (Figure 3C). The decrease in cLTMR frequency and increase in the frequency of the novel UMAP cluster suggests that cLTMR neurons are undergoing expression changes following Nav1.7 knockout that redefine the cLTMR cluster into the novel UMAP cluster. This novel cluster expresses previously described cLTMR markers such as *Th* and *Fam19a4*, though at slightly lower levels (Figure 3D), supporting their identity as modified cLTMR neurons. Other genes normally expressed in cLTMRs show no expression in the new cluster, such as *Ceacam10* (Figure 3D). *Penk*, which is not normally expressed in cLTMRs, shows high expression in the new cLTMR cluster following Nav1.7 knockout (Figure 3D). In the WT DRG, *Penk* shows some expression in a cluster of cold-sensing nociceptors that co-express TRPM8, but the level of *Penk* expression in this cluster does not change following Nav1.7 KO (Figure 3D, lower arrow). The only cells that show increased *Penk* expression following Nav1.7 knockout are in the novel cLTMR cluster.

We verified the expression of *Penk* in cLTMRs by using two-color *in situ* hybridization (ISH)/immunohistochemical (IHC) staining of WT and Nav1.7 KO DRG slices (from lumbar DRGs). To verify that Nav1.7 was properly removed from the Nav1.7 KO DRGs that were used in this analysis, we first performed Nav1.7 ISH (red) with *Penk* ISH (green) and observed complete loss of Nav1.7 expression from all neurons while WT DRGs showed expression in 95% of neurons as expected (Figures S5A–S5D). *Penk* was stained using ISH (red) while the cLTMR marker *Th* was stained using an anti-*Th* antibody (green) (Figures 4A and 4B). In WT DRGs, we find occasional *Penk* expression in very small-diameter neurons that do not express *Th* (Figure 4A). In Nav1.7 KO DRGs, *Penk* is expressed in a large number of medium-diameter neurons, most of which also express *Th*, confirming the scRNA-seq data (Figure 4B). Histogram analysis shows the expression of *Penk* in small/medium-diameter neurons showing the same size distribution as expected for *Th*+ cLTMRs (Figure 4D). The data suggest that approximately 50% of cLTMRs start expressing *Penk* following Nav1.7 KO.

Specific removal of Nav1.7 from cLTMRs does not induce analgesia

To further demonstrate that *Penk* is specifically upregulated in cLTMR neurons, we constructed a conditional Nav1.7 KO mouse where Nav1.7 was removed only from cLTMRs using the vGlut3.cre mouse (Nav1.7 fl/fl;vGlut3.cre). We validated the vGlut3.cre allele by utilizing a tdTomato fl/fl;vGLUT3.cre mouse (Figure S6), showing 90% of cLTMRs labelled with tdTomato. We also demonstrated that Nav1.7 is still expressed in the majority of DRG neurons in the Nav1.7 fl/fl;vGlut3.cre mouse, while neurons that overexpress *Penk* lack Nav1.7 expression as expected (Figures S5E–S5G). We next performed scRNA-seq analysis to compare Nav1.7 fl/fl;vGlut3.cre DRGs with WT (cre.neg)

(C) Analysis of frequencies of neuronal cell types from the DRG. Neuronal cell types show similar frequencies between WT and Nav1.7 KO with the exception of cLTMR WT and cLTMR KO (the novel UMAP cluster that appears in the Nav1.7 KO). N = 6 mice per genotype, Student's t test *$p < 0.01$.
(D) WT and Nav1.7 KO UMAPs showing expression of tyrosine hydroxylase (*Th*), *Ceacam10*, and *Penk*. *Penk* is expressed in Nav1.7 KO cLTMRs as well as cold-sensing DRG neurons (both WT and Nav1.7 KO).

Please cite this article in press as: Deng et al., Nav1.7 is essential for nociceptor action potentials in the mouse in a manner independent of endogenous opioids, Neuron (2023), https://doi.org/10.1016/j.neuron.2023.05.024

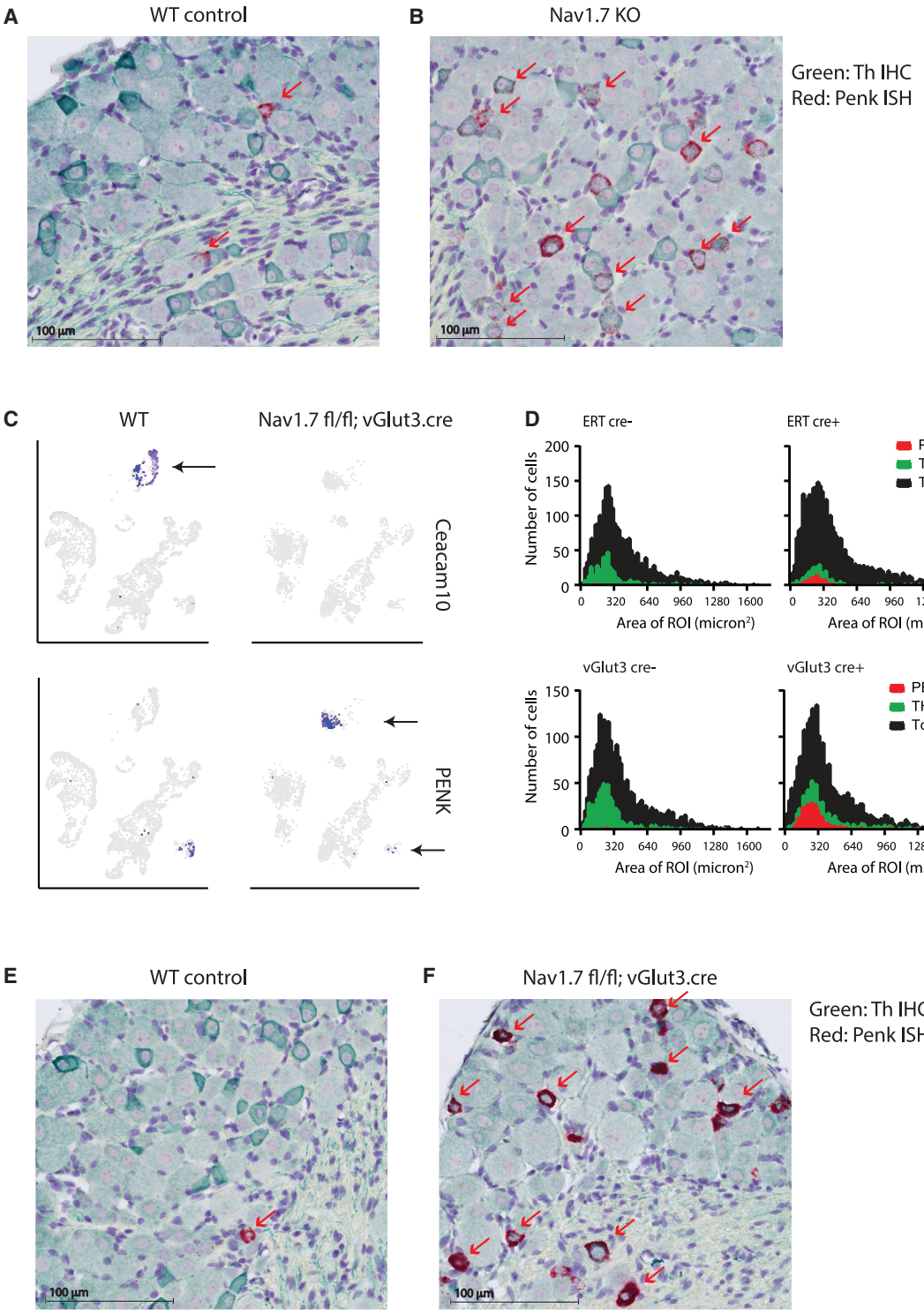

Figure 4. *In situ* hybridization (ISH) analysis of *Penk* + DRG neurons

(A) ISH of WT DRG shows expression of *Penk* in a small number of small-diameter DRG neurons (red arrows) that do not co-stain with *Th*.

(B) ISH of Nav1.7 KO DRGs shows expression of *Penk* in a large number of medium-diameter DRG neurons that also stain for *Th* (IHC) (red arrows).

(C) WT and Nav1.7 fl/fl; vGlut3.Cre DRGs showing expression of *Ceacam10* in cLTMRs (only in WT) and *Penk* expression in cTLMRs (only in KO) and cold-sensing DRG neurons (WT and KO) (indicated by arrows).

(legend continued on next page)

littermate DRGs. UMAP analysis demonstrates the same expression changes in cLTMRs that were found in the full TAM-inducible Nav1.7 KO DRGs, including the appearance of the modified cLTMR cluster and a decrease in the number of cells in the WT cLTMR cluster (Figures S7A–S7D). Expression analysis of DRGs from these mice shows that removal of Nav1.7 from cLTMRs is sufficient to generate the full increase in *Penk* expression and decrease in *Ceacam10* expression as is observed with DRGs from the full Nav1.7 KO (Figures 4C and S5E–S5G). Two-color ISH/IHC staining of WT and Nav1.7 fl/fl;vGlut3.cre mice shows a similar increase in the expression of *Penk* in *Th*+ medium-diameter DRG neurons as was observed in the full (inducible) Nav1.7 KO mouse (Figures 4E and 4F). Histogram analysis shows that approximately 50% of cLTMRs express *Penk* in this cLTMR-specific Nav1.7 KO mouse, similar to what was observed in the full Nav1.7 KO (Figure 4D). We then determined the pain phenotype of the cLTMR-specific Nav1.7 KO mouse (Figure 5). As a positive control, we also examined the full TAM-inducible Nav1.7 KO (8 weeks post-TAM) side by side. We found that while the full Nav1.7 KO mouse showed the expected analgesic phenotype in multiple pain models including Hargreave's, hot plate, tail flick, and tail pinch (Randall-Selito), no analgesic phenotype was observed in the cLTMR-specific Nav1.7 KO, indicating that the upregulation of *Penk* and the downregulation of *Ceacam10* and other cLTMR genes do not significantly impact pain behavior, at least in these nociception models (Figure 5).

Genetic removal or pharmacological block of Nav1.7 suppresses AP-dependent blood flow increases in the hind paw

It has recently been suggested that Nav1.7 KO mice show normal noxious stimulus-induced nociceptor AP generation, suggesting that failure to release neurotransmitter in the spinal cord (and not AP generation/propagation) is responsible for the analgesic phenotype of Nav1.7 KO mice.[24] We used LSCI (laser speckle contrast imaging) to examine AP generation (using blood flow as an indirect measurement) in the skin on the dorsum of the hind paw. Nociceptor APs were initiated by topical application of AITC to the dorsum of one hind paw and vehicle (mineral oil) to the contralateral hind paw as a control (Figure 6A). Following a brief movement artifact that occurs during the application process, the paw treated with AITC showed an increase in blood flow while the vehicle treated paw showed no significant change (Figure 6B). The time course of the LSCI response to AITC has two parts, an initial transient peak lasting for about 1 min followed by a steady tail response (Figure 6C). Both responses fail to develop in TRPA1 (transient receptor potential ankyrin-repeat 1) KO mice, where the receptor for AITC has been removed (Figures 6D and 6E). We found that in comparison with WT mice, Nav1.7 KO mice lack the transient part of the AITC LSCI response but retain the TRPA1-dependent tail response (Figure 6F). This suggests that AP generation in TRPA1-expressing nociceptor fibers in the skin is driving calcium influx and subsequent neuropeptide release and that these APs require Nav1.7. Quantification by measuring the area under the curve (AUC) of the peak AITC response suggests that approximately 50% of TRPA1-dependent blood flow increase is dependent on Nav1.7-mediated APs (Figure 6G). We also performed an experiment on WT mice using GNE-3656 to inhibit Nav1.7 channels to see whether Nav1.7-dependent APs could be inhibited 1 h after dosing. GNE-3565 specifically inhibited the peak AITC response without affecting the tail response in a dose-dependent manner with an EC_{50} = 1 μM (total plasma concentration), suggesting that Nav1.7 inhibition with a selective peripherally restricted inhibitor is sufficient to block Nav1.7-dependent AP generation in the hind paw (Figures 6H–6J).

Pharmacological block of Nav1.7 suppresses C-fiber AP frequency and decreases C-fiber latency without affecting A-fibers

While AITC-induced blood flow changes suggest that Nav1.7 is required for nociceptor AP generation in the skin, we wanted to measure C-fiber APs directly. *In vivo* electrophysiology was used to record the activity of spinal lamina III and IV WDR (wide dynamic range) neurons that receive synapses from sensory neurons innervating the hind paw. Briefly, a microelectrode was inserted into the dorsal horn (lamina III-IV) of the exposed spinal cord of a laminectomized WT C57Bl6 mouse under isoflurane anesthesia to obtain an extracellular single unit recording. For each spinal neuron recording, the receptive field was characterized using a variety of noxious and non-noxious mechanical and thermal stimuli (examples Figures S8A, S8B, S8E, and S8F; compiled data: Figure S8B). Electrical stimulation was then applied to the hind paw every 20 s to separate the spinal APs generated by the recruitment of A-fiber and C-fiber DRG neurons, based on latencies (referred to as A- and C-fiber related APs, respectively) (Figures 7A, S8C, S8D, S8G, and S8H). Raster plots showing the number of APs by latency from successive electrical stimulations show that the number and conduction velocity of A-fiber and C-fiber APs was stable over the period of recording following vehicle injection (Figures 7A, S8C, and S8D). Dosing mice with GNE-3565 (i.v.) caused a sharp decline in BP (measured within the carotid artery). To avoid major changes in BP that could affect the electrophysiological recordings, an automated system was developed to continually monitor BP and automatically inject small boluses of phenylephrine whenever the BP decreased past a set threshold (Figure S10). Perfusing the mice with GNE-3565 (i.v.) at 10 mg/kg while clamping BP in this manner caused an increase in C-fiber, but not A-fiber, latency times and an eventual loss of C-fiber related APs (Figure 7B). The number of C-fiber related action potentials declined over time following GNE-3656 injection in a dose-dependent manner, whereas no significant change in the number of A-fiber related APs was observed (Figures 7C–7E, S9E, S9F, and S9H). The mean latency also increased in a

(D) Stacked histograms showing expression of *Penk* (red) and *Th* (green). Note that *Penk*+ neurons also co-stain with *Th*. Histograms on the left are from WT mice whereas histograms on the right are from Nav1.7 KO mice (either ERT.cre or vGLUT3.cre) (n = 3 mice per genotype).
(E) ISH of WT DRG shows expression of *Penk* in a small number of small-diameter DRG neurons (red arrows).
(F) ISH of Nav1.7 fl/fl; vGLUT3.Cre DRGs shows expression of *Penk* in a large number of medium-diameter DRG neurons that also stain for *Th* (IHC) (red arrows).

Please cite this article in press as: Deng et al., Nav1.7 is essential for nociceptor action potentials in the mouse in a manner independent of endogenous opioids, Neuron (2023), https://doi.org/10.1016/j.neuron.2023.05.024

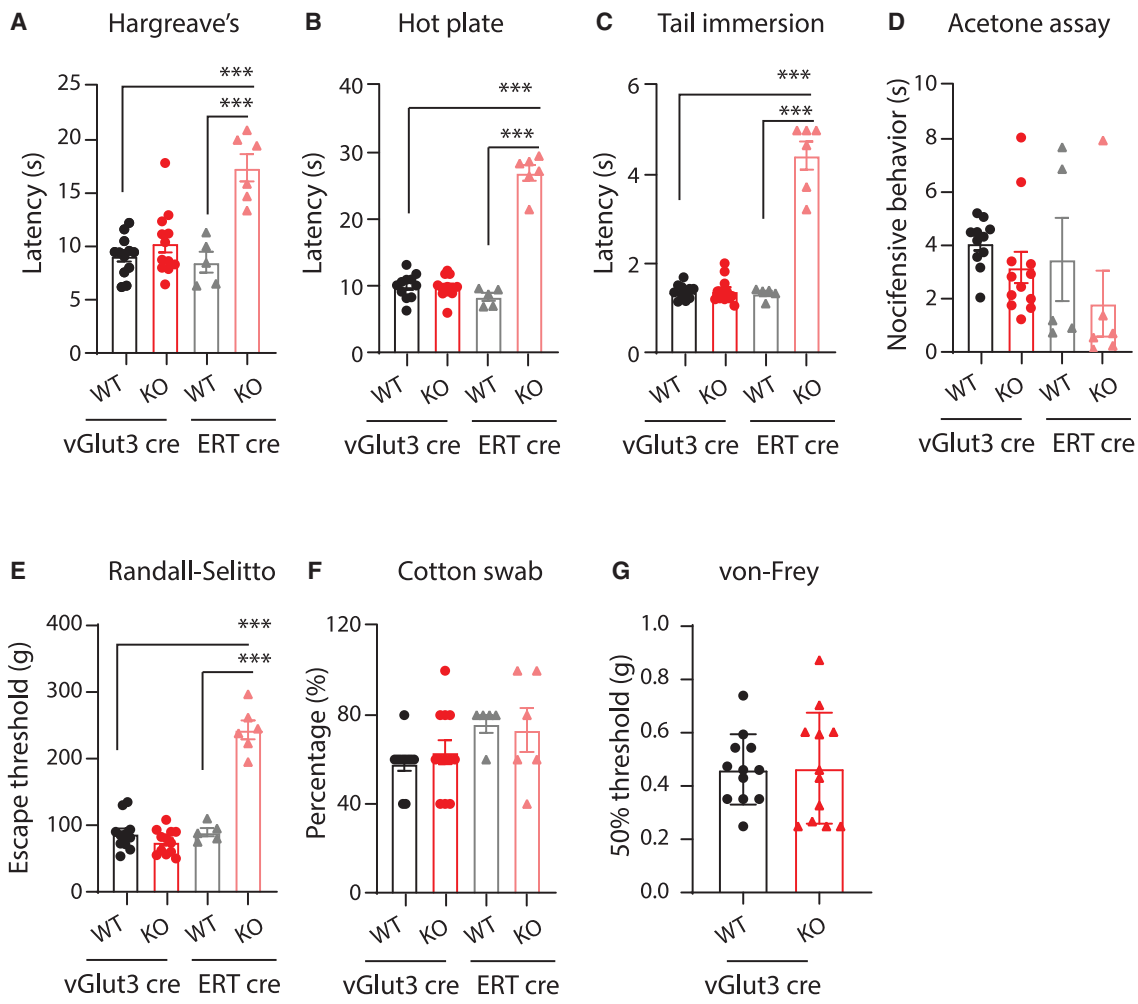

Figure 5. Behavioral analysis of Nav1.7 fl/fl; vGLUT3.cre mice vGLUT3.cre mice are compared with ERT.cre mice

WT is shown in black and KO is shown in red. N = 5–12 mice per group, one-way ANOVA analysis with Tukey's post-hoc multiple comparisons test was performed. ***$p < 0.001$.

(A) Hargreave's test.

(B) Hot plate test.

(C) Tail immersion test.

(D) Acetone test of cold sensitivity (no significant effect of genotype).

(E) Randall-Sellito test of mechanical pressure on the tail.

(F) Cotton-swab test of light mechanical touch (hairy skin next to hind paw) (no significant effect of genotype).

(G) von Frey threshold of mechanical sensitivity to the hind paw (no significant effect of genotype).

dose-dependent manner (Figures 7C–7E and S9G). Such increases in C-fiber latency suggest that inhibition of Nav1.7 is directly affecting AP conduction velocity in C-fibers but not A-fibers. After electrical stimulation was no longer able to elicit APs following GNE-3565 infusion, we found that APs in response to noxious stimuli were also inhibited compared to mice infused with vehicle (Figure S9C), consistent with the effects of GNE-3565 on pain behavior.

Opioid receptor activation in the spinal cord could in theory be responsible for the decrease in the number of observed spinal APs (though not the observed decrease in latency). Indeed, we observe that spinal infusion of morphine, a mu-opioid receptor agonist, inhibits C-fiber-related spinal APs generated by noxious electrical stimulation of the receptive field (Figure 7F). As expected, this opioid-dependent decrease in action potential number could be reversed by i.v. administration of naloxone (3 mg/kg), an inhibitor of mu-opioid receptors (Figure 7F). To determine whether opioid receptors could be involved in the observed decrease in AP frequency following GNE-3565 administration, we dosed i.v. naloxone after APs had been fully inhibited. Naloxone had no effect on the GNE-3565 mediated inhibition of C-fiber related APs, suggesting that opioid receptor activation is not required for Nav1.7-inhibition dependent decreases in AP frequency or increases in latency (Figures 7G and 7H).

Since GNE-3565 is not perfectly selective for Nav1.7, we dosed Nav1.7 MBS mice to demonstrate that the observed effects of

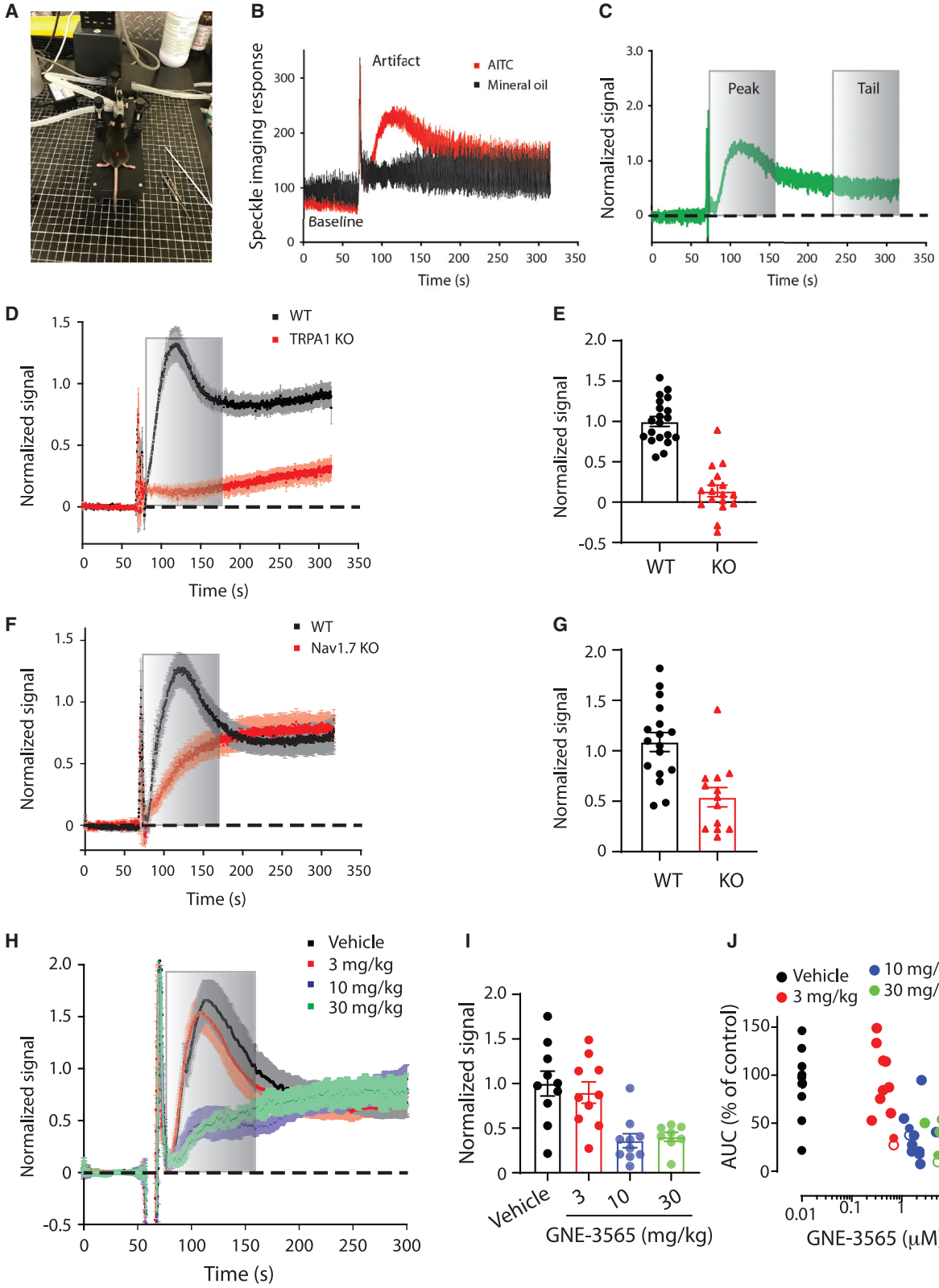

(legend on next page)

Please cite this article in press as: Deng et al., Nav1.7 is essential for nociceptor action potentials in the mouse in a manner independent of endogenous opioids, Neuron (2023), https://doi.org/10.1016/j.neuron.2023.05.024

GNE-3565 on C-fiber related APs were indeed due specifically to block of Nav1.7. Accordingly, i.v. infusion of GNE-3565 into the Nav1.7 MBS mouse failed to alter C-fiber latency or AP frequency while infusion of GNE-3565 into WT littermate mice showed the previously observed increase in C-fiber latency and decrease in AP frequency (Figures 7I and 7J; example recordings: WT, Figures S11A–S11D; Nav1.7 MBS Figures S11E–S11H; compiled data: Figure S12). This shows that the observed effects of GNE-3565 on C-fiber latency, AP frequency, and stimuli-induced APs are indeed due to block of Nav1.7 channels.

Recordings from WDR spinal neurons illustrate the resulting input from multiple C-fiber and A-fiber sensory neurons simultaneously. However, these recordings cannot strictly differentiate the effects of blocking Nav1.7 channels on nociceptors at the peripheral (transduction and conduction) vs. central (synaptic transmission) levels. We therefore performed extracellular single unit recordings within the DRG using the same setup that was used for individual spinal neuron recording. Electrical stimulation of the hind paw was used to identify individual nociceptors with unmyelinated distal axons (i.e., C-fibers), characterized by conduction velocity <2.5 m/s (Figure 8A). In addition, each recorded C-fiber neuron was characterized using the same set of noxious and non-noxious mechanical and thermal stimuli used for spinal neuron characterization (examples: Figures S13A, S13E, and S13I; compiled data: Figures S14A–S14C). Focusing on unmyelinated nociceptors, we found that i.v. infusion of GNE-3565 resulted in decreased AP conduction velocity, supporting that the corresponding increase in C-fiber related AP latencies observed at the spinal cord level originated at the peripheral level (Figure 8B). To show that this effect was specific to inhibition of Nav1.7, responses from unmyelinated nociceptors from Nav1.7 MBS mice and WT littermate were compared during GNE-3565 infusion. Only C-fiber nociceptors from WT mice showed increased AP latency in response to electrical stimulation of the receptive field following GNE-3565 perfusion (Figure 8B). WT mouse AP latency increased by 35% on average vs. 0% for Nav1.7 MBS mouse (Figure 8C). In addition, most WT C-fiber nociceptors failed to respond to electrical stimulation of the receptive field after some period of time following the start of GNE-3565 perfusion, an effect that did not occur in the Nav1.7 MBS mice (Figure 8D). At the end of all recordings, each C-fiber nociceptor was tested using its preferred stimulation type (50°C, pinch, or 0°C, defined during the initial characterization using the full range of stimulation). WT C-fiber nociceptors no longer fired APs to the preferred stimulus following GNE-3565 perfusion (with the exception of a single cold-sensing fiber), while Nav1.7 MBS C-fibers showed no change in AP number after the preferred stimulus (examples Figures S13B, S13C, S13F, S13G, S13J, and S13K; compiled data: Figure S14D).

In some cases, we observed that after a C-fiber neuron stopped responding to electrical stimulation of the receptive field upon GNE-3565 injection, increasing the intensity of the electrical stimulation led to recovery of AP generation (Figure 8E). In this example, increasing the level of stimulation intensity after the C-fiber became unresponsive allowed recovery of the recorded AP multiple times (arrows) following GNE-3565 infusion. Eventually, the neuron no longer responded even when the stimulation was set to the maximum level (10 mA, 0.2 ms duration). This suggests that initiation of APs at the fiber endings in the hind paw is more sensitive to Nav1.7 inhibition than propagation of APs in the sciatic nerve. To examine this further, responses of spinal WDR neurons to alternate electrical stimulations of the hind paw and sciatic nerve were recorded. Following GNE-3656 i.v. infusion, AP latency increased, and the number of action potentials decreased with hind paw electrical stimulations, as observed before (Figure 8F). However, the number of APs did not significantly decrease with direct sciatic nerve stimulation, though there was an increase in C-fiber latencies (Figures 8F–8H).

DISCUSSION

It has recently been suggested that overexpression of *Penk* in DRG neurons that occurs in the Nav1.7 KO mouse is responsible for the observed CIP-like analgesia.[23,24] The hypothesis is that in the absence of Nav1.7 expression, DRG neurons overexpress *Penk* and release enkephalin peptide into the dorsal horn of the spinal cord, suppressing neurotransmitter release by nociceptors. In this manner, Nav1.7 would not strictly be required for nociceptor AP generation as was originally proposed but instead would be required for maintaining low levels of expression of *Penk* in the DRG. Our data suggest that *Penk* expression in the DRG is indeed increased after genetic removal of Nav1.7, but we find no evidence that this increase in *Penk* plays any role in the analgesia observed following genetic removal of Nav1.7 or inhibition of Nav1.7 by a selective inhibitor. Our results call into question the enkephalin hypothesis and are as follow: (1) GNE-3565, a selective inhibitor of Nav1.7, induces analgesia within 1 h after oral dosing, faster than expected for a process requiring overexpression of *Penk*, transport of enkephalin to the spinal cord, and release into the spinal cord, and in fact prior to any observed increase in *Penk* expression; (2) dosing mice with naloxone following TAM-induced genetic removal of Nav1.7 fails

Figure 6. Laser speckle contrast imaging (LSCI) of hind paw after AITC application

(A) LSCI setup showing anesthetized mouse on a warm plate with hind paws positioned dorsal side up.
(B) Raw LSCI waveform following AITC application on one hind paw and mineral oil application on the other hind paw. Spike-like artifact is due to brief movement while applying AITC/mineral oil.
(C) Vehicle subtracted LSCI waveform showing transient peak response and tail response to AITC.
(D) Average LSCI waveform between WT (black) and TRPA1 KO mouse (red).
(E) Quantification of area under the curve (AUC) during the peak response window (n = 19 mice per genotype).
(F) Average LSCI waveform between WT (black) and Nav1.7 KO mouse (red).
(G) Quantification of AUC during the peak response window (n = 13–17 mice per genotype).
(H) Average LSCI waveform after dosing mice with vehicle (black) or 3 mg/kg (red), 10 mg/kg (purple), or 30 mg/kg (green) GNE-3565.
(I) Quantification of LSCI waveform showing peak of the response for individual mice at difference doses of GNE-3565 (n = 10 mice per group).
(J) Quantification of LSCI waveform showing AUC for individual mice at difference doses of GNE-3565.

Please cite this article in press as: Deng et al., Nav1.7 is essential for nociceptor action potentials in the mouse in a manner independent of endogenous opioids, Neuron (2023), https://doi.org/10.1016/j.neuron.2023.05.024

CellPress
OPEN ACCESS

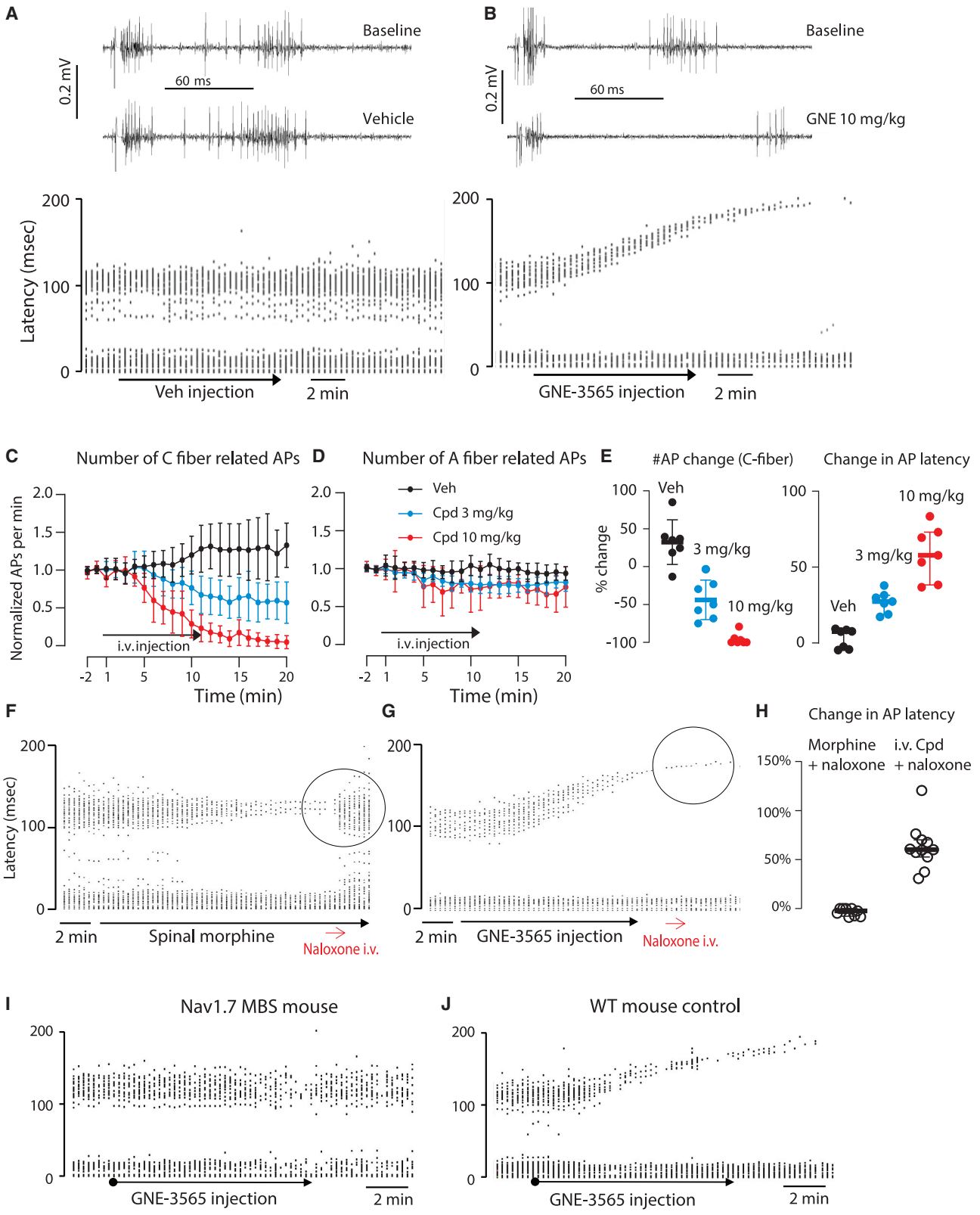

(legend on next page)

Please cite this article in press as: Deng et al., Nav1.7 is essential for nociceptor action potentials in the mouse in a manner independent of endogenous opioids, Neuron (2023), https://doi.org/10.1016/j.neuron.2023.05.024

to reverse the observed analgesia in multiple models of nociception; (3) the increase in *Penk* expression that occurs after TAM-induced removal of Nav1.7 is specific for cLTMRs, and genetic removal of Nav1.7 from cLTMRs does not result in analgesia despite similar increases of *Penk* expression in the DRG as observed in the full TAM-inducible KO mouse; (4) the decreased frequency and increased latency of C-fiber related APs following i.v. infusion of GNE-3565 is not reversed by i.v. infusion of naloxone, whereas the morphine-induced decrease in C-fiber related APs is sensitive to naloxone as expected.

It is not clear why our results differ from those of Minett et al.[23] One possibility is that our experiments were done using either a selective inhibitor of Nav1.7 or a TAM-inducible Nav1.7 KO mouse where Nav1.7 is genetically removed in the adult, whereas Minett et al.[23] used an advillin.cre tissue-specific Nav1.7 KO mouse that removes Nav1.7 much earlier during development. Our approach thus avoids potential developmental compensation that could occur when mice undergo embryonic and early post-natal development without Nav1.7. Overall, our data clearly suggest that the analgesia resulting from inhibition or genetic removal of Nav1.7 in the adult is not dependent on *Penk* overexpression or μ-opioid activation.

We found that the observed Nav1.7-removal dependent overexpression of *Penk* occurs specifically in cLTMR DRG neurons. These sensory neurons are thought to play a role in pleasant touch and are not considered nociceptors, even though they are non-myelinated C-fibers. It has recently been established that Nav1.7 is required for cLTMR function in both mice and humans,[30] and this is consistent with our study showing effects on gene expression in cLTMRs following genetic removal of Nav1.7. Our hypothesis is that cLTMR gene expression is activity dependent, and when cLTMRs are silenced by removal of Nav1.7, activity-dependent gene expression is modified. Under baseline conditions when the mice are living in their cages (where primarily low-threshold stimuli are present), cLTMRs are the only Nav1.7-dependent C-fiber neurons that are consistently firing APs, explaining why such activity-dependent changes in gene expression after Nav1.7 removal are specific to this class of DRG neuron.

It has recently been suggested that C-fiber APs do not depend of Nav1.7 function *in vivo* and that the analgesia phenotype observed in Nav1.7 KO mice is due to suppression of neurotransmitter release in the dorsal horn of the spinal cord.[24] Other literature suggests that 2/3 of nociceptors require Nav1.7 *in vivo* for nociceptor AP propagation.[31] A recent study in the cynomologous macaque showed that selective Nav1.7 inhibitors were able to slow C-fiber AP velocity and eventually block C-fiber APs (but not A-fiber APs) in 100% of fibers tested.[32] Our *in vivo* electrophysiology studies show that the selective Nav1.7 inhibitor GNE-3565 slows C-fiber AP velocity and blocks C-fiber APs following i.v. infusion while A-fiber APs are not affected. We observe C-fiber AP block in both WDR dorsal horn single unit recordings, where we can observe multiple A-fibers and C-fibers synapsing onto a single WDR neuron, and DRG C-fiber single unit recordings, where C-fiber APs can be recorded directly. Our results are comparable to Kraus et al.[32] but different from MacDonald et al.[24] A few experimental differences between our study and MacDonald et al.[24] should be noted. (1) We used a selective Nav1.7 inhibitor in our studies, whereas MacDonald et al.[24] used a DRG-specific Nav1.7 KO mouse. The advantage of using a selective inhibitor is that we can observe C-fiber APs both before and after drug infusion to guarantee that we have established a good quality C-fiber recording prior to C-fiber AP block. In addition, experiments with a selective inhibitor avoid potential complications due to developmental compensation that might occur when Nav1.7 is removed during early development. To verify that our selective inhibitor was in fact showing its effects by blocking Nav1.7, we employed the Nav1.7 MBS mouse. These experiments clearly show that C-fiber APs are dependent on Nav1.7 function in the adult. (2) In our experiments, we used single unit recordings in the DRG and spinal cord for our analysis whereas MacDonald et al.[24] used either calcium imaging or multi-unit electrical recordings. Such multi-unit recordings will record from many fibers, including A-fibers that are not Nav1.7 dependent. MacDonald et al.[24] made no attempt to verify that the fibers they recorded were C-fibers.

Our data clearly demonstrate that C-fiber APs are dependent on Nav1.7. However, we wanted to determine at which step the Nav1.7 dependency occurs, which could be the initiation of APs at fibers in the skin, the propagation of APs down the nerve, or the secretion of neurotransmitter in the spinal cord. Our data clearly suggest that Nav1.7 plays a major role in the initiation of APs in the skin. The LSCI experiments, which measures AP-dependent blood flow in the skin of the hind paw and is only sensitive to APs near/within the skin at the initiation site, clearly suggest that initiation of APs is Nav1.7 dependent. These skin APs

Figure 7. *In vivo* electrophysiological analysis of sensory neuron Aps and effects of GNE-3565

(A) Single unit WDR dorsal horn neuron recordings after electrical stimulation of the hind paw. Spinal neuron APs reflect pre-synaptic sensory neuron Aps (above). A-fiber and C-fiber related APs shown by latency-time raster plot (below). Vehicle i.v. infusion does not show an effect.

(B) Single unit WDR recording showing the effects of 10 mg/kg GNE-3565 infusion. Drug infusion causes an increase in C-fiber related AP latencies and an eventual decrease in AP frequency.

(C) Number of C-fiber related APs per min. following i.v. infusion of vehicle, 3 mg/kg, or 10 mg/kg GNE-3565.

(D) Number of A-fiber related APs per min.

(E) Percent change in the number of C-fiber related APs and C-fiber AP latency after i.v. infusion of GNE-3565 (or vehicle). Data points represent average change for each individual mouse (n = 7 mice per group).

(F) Single unit WDR recording showing the effect of local spinal application of morphine (decrease in C-fiber related APs and rescue by i.v. naloxone).

(G) Single unit WDR recording showing the effect of i.v. infusion of 10 mg/kg GNE-3565 (increase in C-fiber related latency and decrease in AP number). i.v. naloxone failed to rescue latency increase or AP number changes.

(H) Change in AP latency following morphine vs. GNE-3565 (n = 10 mice per group).

(I) Single unit WDR recording showing no effects of 10 mg/kg GNE-3565 on AP latency in the Nav1.7 modified binding site (MBS) mouse.

(J) Control experiment done side by side on WT mouse (vs. MBS mouse).

Please cite this article in press as: Deng et al., Nav1.7 is essential for nociceptor action potentials in the mouse in a manner independent of endogenous opioids, Neuron (2023), https://doi.org/10.1016/j.neuron.2023.05.024

CellPress
OPEN ACCESS

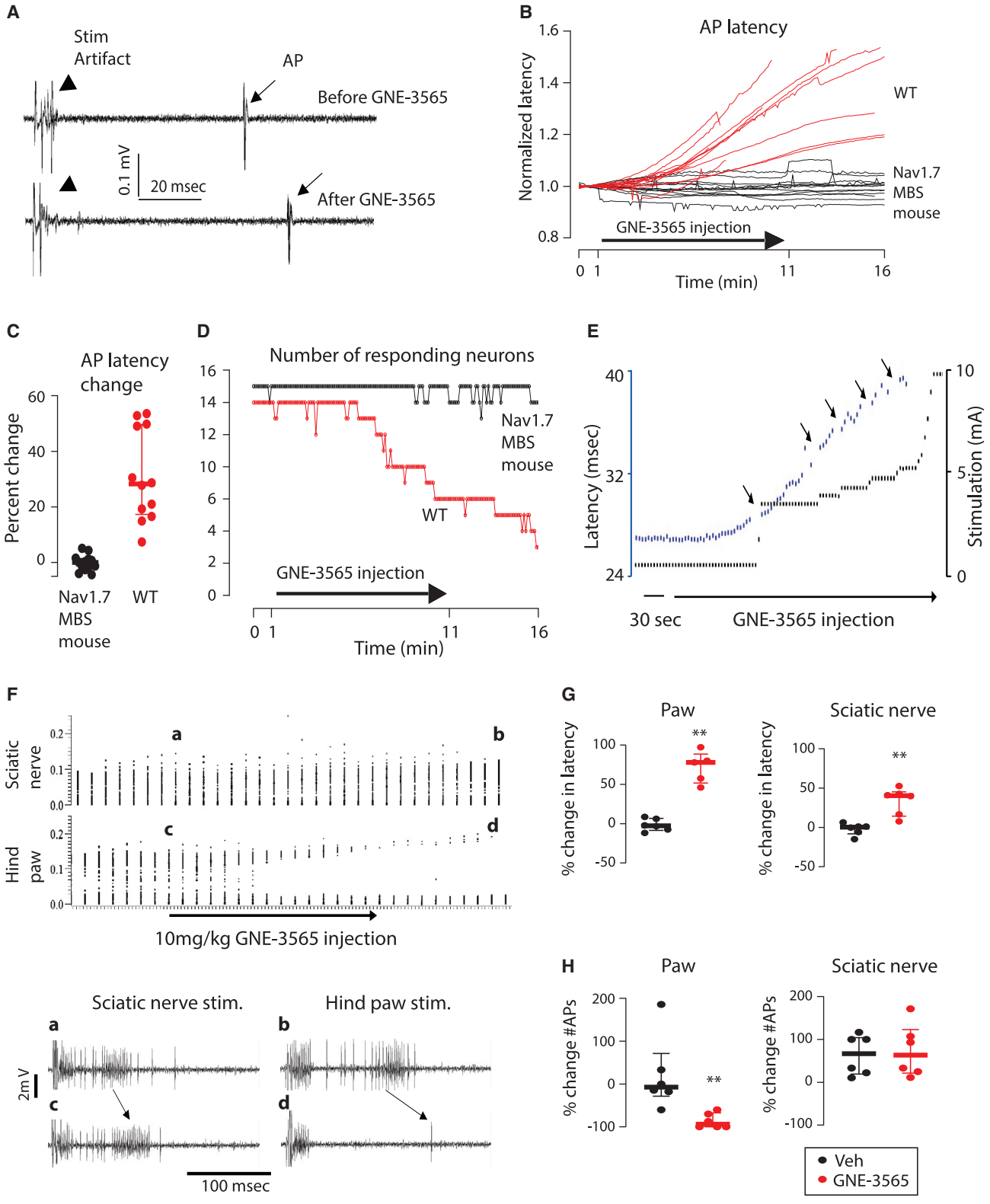

(legend on next page)

Please cite this article in press as: Deng et al., Nav1.7 is essential for nociceptor action potentials in the mouse in a manner independent of endogenous opioids, Neuron (2023), https://doi.org/10.1016/j.neuron.2023.05.024

(as measured indirectly by blood flow) can be blocked by either genetic removal of Nav1.7 or selective inhibition of Nav1.7. We also found that C-fiber APs, after being blocked by GNE-3565, could sometimes be rescued by increasing the amplitude of electrical stimulation to the hind paw, again suggesting that initiation of APs (which is dependent on the amplitude of electrical stimulation at the paw) is more sensitive to Nav1.7 inhibition than propagation. Finally, when we directly stimulated the sciatic nerve, we no longer observed block of C-fiber APs by GNE-3565, suggesting that initiation/propagation of APs in the nerve is less sensitive to Nav1.7 block than initiation in the skin. This suggests that once APs are initiated, other Nav channels such as Nav1.8 allow propagation of C-fiber APs in the absence of functional Nav1.7 channels, albeit with slower C-fiber AP velocity.

It has been suggested that the observed lack of clinical efficacy of selective Nav1.7 inhibitors suggests that we lack understanding of the function of Nav1.7 in the transmission of nociceptive information.[31,33] However, the only selective Nav1.7 inhibitor thus far tested in the clinic for efficacy has been PF-05089771. Despite the high potency of this compound, it has been found unable to achieve sufficient coverage of the Nav1.7 IC50 to effectively engage the target *in vivo* in both rodents and non-human primates.[29,32] Such lack of target engagement and efficacy has been observed even with the highly potent aryl-sulfonamide PF-06456384, which is >100-fold more potent than PF-05089771.[34] It is not clear why these potent inhibitors are not able to achieve *in vivo* target engagement, but aryl-sulfonamides of this class have poor drug-like properties and are highly bound to plasma proteins (>99.99% bound) *in vivo*. Newer-generation inhibitors with zwitterionic character, such as GNE-3565 described in this paper, Merck's SSCI-1,[32] and GDC-0276,[35] are able to achieve a higher level of target engagement and CIP-like efficacy in pain models. Unfortunately, such molecules have not yet been tested for efficacy in clinical trials, in part due to severe autonomic side effects observed in pre-clinical safety studies, particularly in non-rodent studies. One example of an observed autonomic side effect in humans has been Nav1.7-inhibitor-dependent decrease in BP.[35] We observed a similar effect on BP in mice following i.v. infusion of GNE-3565, which we can demonstrate is on-target and due to Nav1.7 blockade (Figures S10B–S10F). Our data suggest that Nav1.7 inhibitors with sufficient *in vivo* target engagement will show high levels of efficacy in clinical trials as expected for a drug that can suppress C-fiber APs, though safety issues due to effects on the autonomic nervous system could be limiting.

STAR★METHODS

Detailed methods are provided in the online version of this paper and include the following:

- KEY RESOURCES TABLE
- RESOURCE AVAILABILITY
  - Lead contact
  - Materials availability
  - Data and code availability
- EXPERIMENTAL MODEL AND STUDY PARTICIPANT DETAILS
  - Mouse and mouse lines
  - Generation of SCN9A YWV→SRL KI mouse
  - Generation of SCN8A YW→SR KI mouse
- METHOD DETAILS
  - Quantitative PCR (qPCR)
  - Dynaflow patch clamp recording
  - In vitro field stimulation and calcium imaging
  - In vivo electrophysiological recording
  - Bulk RNAseq
  - Single cell RNAseq
  - Single nuclei sequencing
  - Immunohistochemistry
  - In situ hybridization
  - Pain behavioral assays
  - Randal Sellito
  - Hargreave's test
  - Acetone evaporation test
  - Von Frey hair test
  - Hot plate test
  - Tail immersion test
  - Cotton wisp test
  - Open field test for spontaneous locomotor function
  - Blood pressure measurement with the CODA tail cuff method
  - Laser speckle contrast imaging
  - Properties and dosing of GNE-3565
  - Synthesis of GNE-3565
- QUANTIFICATION AND STATISTICAL ANALYSIS

Figure 8. *In vivo* electrophysiological analysis of sensory neuron APs and effects of GNE-3565 part 2

(A) C-fiber DRG neuron recording showing single APs induced by electrical stimulation of the hind paw before and after 10 mg/kg GNE-3565 infusion.

(B) AP latency measurements from single unit DRG C-fiber recordings over time during and after infusion of GNE-3565. WT neurons (WT) showed increased latency while Nav1.7 MBS neurons (black) showed no effect.

(C) AP latency change following GNE-3565 infusion. Data points represent average latency change for each individual mouse. AP latency was significantly increased following infusion in WT but not Nav1.7 MBS mice ($p < 0.001$, Mann-Whitney test, $n = 12$ mice per group).

(D) Number of responding DRG neurons following 10 mg/kg GNE-3565 infusion.

(E) AP latency (left y axis) of a mechano-specific C-fiber DRG neuron induced by hind paw stimulation (intensity of electrical stimulation, right y axis). Electrical stimulation failed to initiate APs (arrows) as GEN-3565 exposure increased. APs could be rescued by increasing stimulation intensity (up to 10 mA).

(F) Single unit WDR recording showing the effects of 10 mg/kg GNE-3565 on AP latency. APs were elicited either by direct sciatic nerve stimulation (above) or hind paw stimulation (below).

(G) Quantification showing significant increase in AP latency following infusion of GNE-3565 (red) vs. vehicle (black). $^{**}p < 0.01$ (Mann-Whitney test, $n = 6$ mice per group).

(H) Quantification showing significant decrease in AP number only with paw stimulation following infusion of GNE-3565 (red) vs. vehicle (black). $^{**}p < 0.01$ (Mann-Whitney test, $n = 6$ mice per group).

SUPPLEMENTAL INFORMATION

Supplemental information can be found online at https://doi.org/10.1016/j.neuron.2023.05.024.

ACKNOWLEDGMENTS

We are grateful for the help from Yuxin Liang, Qixin Bei, and Zora Mordrusan for next-generation DNA sequencing support, and the laboratory animal research core for supporting our mouse experiments.

AUTHOR CONTRIBUTIONS

L.D., M.D., R.M.R., S.D.S., J.M., H.L., O.F., J.T., H.N., V.J., S.L., L.S.O., P.K., and J.A. conducted experiments. K.H., M.J., and J.S.K. did computational analyses. M.R.-G. and L.T. generated MBS mice. K.L.S., J.A., and D.H.H. administered the project and wrote the manuscript.

DECLARATION OF INTERESTS

L.D., M.D., R.M.R., S.D.S., J.M., H.L., O.F., H.N., V.J., K.H., M.J., J.S.K., and D.H.H. are employees of Genentech, Inc., a for-profit pharmaceutical company. S.L., L.S.O., P.K., and J.A. declare no competing interests. GNE-3565 is patented by Genentech Inc. and Xenon Pharmaceuticals (US10457654B2), and none of the authors is listed as an inventor.

Received: October 3, 2022
Revised: April 7, 2023
Accepted: May 26, 2023
Published: June 22, 2023

REFERENCES

1. Cox, J.J., Reimann, F., Nicholas, A.K., Thornton, G., Roberts, E., Springell, K., Karbani, G., Jafri, H., Mannan, J., Raashid, Y., et al. (2006). An SCN9A channelopathy causes congenital inability to experience pain. Nature *444*, 894–898. https://doi.org/10.1038/nature05413.
2. Goldberg, Y.P., MacFarlane, J., MacDonald, M.L., Thompson, J., Dube, M.P., Mattice, M., Fraser, R., Young, C., Hossain, S., Pape, T., et al. (2007). Loss-of-function mutations in the Nav1.7 gene underlie congenital indifference to pain in multiple human populations. Clin. Genet. *71*, 311–319. https://doi.org/10.1111/j.1399-0004.2007.00790.x.
3. Cummins, T.R., Dib-Hajj, S.D., and Waxman, S.G. (2004). Electrophysiological properties of mutant Nav1.7 sodium channels in a painful inherited neuropathy. J. Neurosci. *24*, 8232–8236. https://doi.org/10.1523/JNEUROSCI.2695-04.2004.
4. Eberhardt, M., Nakajima, J., Klinger, A.B., Neacsu, C., Hühne, K., O'Reilly, A.O., Kist, A.M., Lampe, A.K., Fischer, K., Gibson, J., et al. (2014). Inherited pain: sodium channel Nav1.7 A1632T mutation causes erythromelalgia due to a shift of fast inactivation. J. Biol. Chem. *289*, 1971–1980. https://doi.org/10.1074/jbc.M113.502211.
5. Han, C., Dib-Hajj, S.D., Lin, Z., Li, Y., Eastman, E.M., Tyrrell, L., Cao, X., Yang, Y., and Waxman, S.G. (2009). Early- and late-onset inherited erythromelalgia: genotype-phenotype correlation. Brain *132*, 1711–1722. https://doi.org/10.1093/brain/awp078.
6. Lampert, A., Eberhardt, M., and Waxman, S.G. (2014). Altered sodium channel gating as molecular basis for pain: contribution of activation, inactivation, and resurgent currents. In Voltage Gated Sodium Channels, P.C. Ruben, ed. (Springer), pp. 91–110. https://doi.org/10.1007/978-3-642-41588-3_5.
7. Choi, J.-S., Boralevi, F., Brissaud, O., Sánchez-Martín, J., Te Morsche, R.H.M., Dib-Hajj, S.D., Drenth, J.P.H., and Waxman, S.G. (2011). Paroxysmal extreme pain disorder: a molecular lesion of peripheral neurons. Nat. Rev. Neurol. *7*, 51–55. https://doi.org/10.1038/nrneurol.2010.162.
8. Dib-Hajj, S.D., Estacion, M., Jarecki, B.W., Tyrrell, L., Fischer, T.Z., Lawden, M., Cummins, T.R., and Waxman, S.G. (2008). Paroxysmal extreme pain disorder M1627K mutation in human Nav1.7 renders DRG neurons hyperexcitable. Mol. Pain *4*, 37. https://doi.org/10.1186/1744-8069-4-37.
9. Estacion, M., Dib-Hajj, S.D., Benke, P.J., Te Morsche, R.H.M., Eastman, E.M., Macala, L.J., Drenth, J.P.H., and Waxman, S.G. (2008). NaV1.7 gain-of-function mutations as a continuum: A1632E displays physiological changes associated with erythromelalgia and paroxysmal extreme pain disorder mutations and produces symptoms of both disorders. J. Neurosci. *28*, 11079–11088. https://doi.org/10.1523/JNEUROSCI.3443-08.2008.
10. Faber, C.G., Hoeijmakers, J.G.J., Ahn, H.-S., Cheng, X., Han, C., Choi, J.-S., Estacion, M., Lauria, G., Vanhoutte, E.K., Gerrits, M.M., et al. (2012). Gain of function Naν1.7 mutations in idiopathic small fiber neuropathy. Ann. Neurol. *71*, 26–39. https://doi.org/10.1002/ana.22485.
11. Payandeh, J., and Hackos, D.H. (2018). Selective ligands and drug discovery targeting the voltage-gated sodium channel Nav1.7. In Handbook of Experimental Pharmacology, M. Chahine, ed. (Springer International Publishing), pp. 271–306. https://doi.org/10.1007/164_2018_97.
12. Hille, B. (2001). Ion Channels of Excitable Membranes, Third Edition (Sinauer).
13. Hodgkin, A.L., and Huxley, A.F. (1952). A quantitative description of membrane current and its application to conduction and excitation in nerve. J. Physiol. *117*, 500–544.
14. Dib-Hajj, S.D., Cummins, T.R., Black, J.A., and Waxman, S.G. (2010). Sodium channels in normal and pathological pain. Annu. Rev. Neurosci. *33*, 325–347. https://doi.org/10.1146/annurev-neuro-060909-153234.
15. Fukuoka, T., Kobayashi, K., Yamanaka, H., Obata, K., Dai, Y., and Noguchi, K. (2008). Comparative study of the distribution of the α-subunits of voltage-gated sodium channels in normal and axotomized rat dorsal root ganglion neurons. J. Comp. Neurol. *510*, 188–206. https://doi.org/10.1002/cne.21786.
16. Vasylyev, D.V., and Waxman, S.G. (2012). Membrane properties and electrogenesis in the distal axons of small dorsal root ganglion neurons in vitro. J. Neurophysiol. *108*, 729–740. https://doi.org/10.1152/jn.00091.2012.
17. Rush, A.M., Dib-Hajj, S.D., Liu, S., Cummins, T.R., Black, J.A., and Waxman, S.G. (2006). A single sodium channel mutation produces hyper- or hypoexcitability in different types of neurons. Proc. Natl. Acad. Sci. USA *103*, 8245–8250. https://doi.org/10.1073/pnas.0602813103.
18. Kohane, D.S., Yieh, J., Lu, N.T., Langer, R., Strichartz, G.R., and Berde, C.B. (1998). A re-examination of tetrodotoxin for prolonged duration local anesthesia. Anesthesiology *89*, 119–131. https://doi.org/10.1097/00000542-199807000-00019.
19. Kornecook, T.J., Yin, R., Altmann, S., Be, X., Berry, V., Ilch, C.P., Jarosh, M., Johnson, D., Lee, J.H., Lehto, S.G., et al. (2017). Pharmacologic characterization of AMG8379, a potent and selective small molecule sulfonamide antagonist of the voltage-gated sodium channel Naν1.7. J. Pharmacol. Exp. Ther. *362*, 146–160. https://doi.org/10.1124/jpet.116.239590.
20. Padera, R.F., Tse, J.Y., Bellas, E., and Kohane, D.S. (2006). Tetrodotoxin for prolonged local anesthesia with minimal myotoxicity. Muscle Nerve *34*, 747–753. https://doi.org/10.1002/mus.20618.
21. Zhao, C., Liu, A., Santamaria, C.M., Shomorony, A., Ji, T., Wei, T., Gordon, A., Elofsson, H., Mehta, M., Yang, R., et al. (2019). Polymer-tetrodotoxin conjugates to induce prolonged duration local anesthesia with minimal toxicity. Nat. Commun. *10*, 2566. https://doi.org/10.1038/s41467-019-10296-9.
22. Isensee, J., Krahé, L., Moeller, K., Pereira, V., Sexton, J.E., Sun, X., Emery, E., Wood, J.N., and Hucho, T. (2017). Synergistic regulation of serotonin and opioid signaling contributes to pain insensitivity in Nav1.7 knockout mice. Sci. Signal. *10*, eaah4874. https://doi.org/10.1126/scisignal.aah4874.
23. Minett, M.S., Pereira, V., Sikandar, S., Matsuyama, A., Lolignier, S., Kanellopoulos, A.H., Mancini, F., Iannetti, G.D., Bogdanov, Y.D., Santana-Varela, S., et al. (2015). Endogenous opioids contribute to insensitivity to pain in humans and mice lacking sodium channel Nav1.7. Nat. Commun. *6*, 8967. https://doi.org/10.1038/ncomms9967.

24. MacDonald, D.I., Sikandar, S., Weiss, J., Pyrski, M., Luiz, A.P., Millet, Q., Emery, E.C., Mancini, F., Iannetti, G.D., Alles, S.R.A., et al. (2021). A central mechanism of analgesia in mice and humans lacking the sodium channel NaV1.7. Neuron *109*, 1497–1512.e6. https://doi.org/10.1016/j.neuron.2021.03.012.

25. Shields, S.D., Deng, L., Reese, R.M., Dourado, M., Tao, J., Foreman, O., Chang, J.H., and Hackos, D.H. (2018). Insensitivity to pain upon adult-onset deletion of Nav1.7 or its blockade with selective inhibitors. J. Neurosci. *38*, 10180–10201. https://doi.org/10.1523/JNEUROSCI.1049-18.2018.

26. Usoskin, D., Furlan, A., Islam, S., Abdo, H., Lönnerberg, P., Lou, D., Hjerling-Leffler, J., Haeggström, J., Kharchenko, O., Kharchenko, P.V., et al. (2015). Unbiased classification of sensory neuron types by large-scale single-cell RNA sequencing. Nat. Neurosci. *18*, 145–153. https://doi.org/10.1038/nn.3881.

27. Li, L., Rutlin, M., Abraira, V.E., Cassidy, C., Kus, L., Gong, S., Jankowski, M.P., Luo, W., Heintz, N., Koerber, H.R., et al. (2011). The functional organization of cutaneous low-threshold mechanosensory neurons. Cell *147*, 1615–1627. https://doi.org/10.1016/j.cell.2011.11.027.

28. Ahuja, S., Mukund, S., Deng, L., Khakh, K., Chang, E., Ho, H., Shriver, S., Young, C., Lin, S., Johnson, J.P., et al. (2015). Structural basis of Nav1.7 inhibition by an isoform-selective small-molecule antagonist. Science *350*, aac5464. https://doi.org/10.1126/science.aac5464.

29. Bankar, G., Goodchild, S.J., Howard, S., Nelkenbrecher, K., Waldbrook, M., Dourado, M., Shuart, N.G., Lin, S., Young, C., Xie, Z., et al. (2018). Selective NaV1.7 antagonists with long residence time show improved efficacy against inflammatory and neuropathic pain. Cell Rep. *24*, 3133–3145. https://doi.org/10.1016/j.celrep.2018.08.063.

30. Middleton, S.J., Perini, I., Andreas, C.T., Weir, G.A., McCann, K., Barry, A.M., Marshall, A., Lee, M., Mayo, L.M., Bohic, M., et al. (2021). Nav1.7 is required for normal C-low threshold mechanoreceptor function in humans and mice. Brain *145*, 3637–3653. https://doi.org/10.1093/brain/awab482.

31. Goodwin, G., McMurray, S., Stevens, E.B., Denk, F., and McMahon, S.B. (2022). Examination of the contribution of Nav1.7 to axonal propagation in nociceptors. Pain *163*, e869–e881. https://doi.org/10.1097/j.pain.0000000000002490.

32. Kraus, R.L., Zhao, F., Pall, P.S., Zhou, D., Vardigan, J.D., Danziger, A., Li, Y., Daley, C., Ballard, J.E., Clements, M.K., et al. (2021). Nav1.7 target modulation and efficacy can be measured in nonhuman primate assays. Sci. Transl. Med. *13*, eaay1050. https://doi.org/10.1126/scitranslmed.aay1050.

33. Eagles, D.A., Chow, C.Y., and King, G.F. (2022). Fifteen years of NaV 1.7 channels as an analgesic target: why has excellent in vitro pharmacology not translated into in vivo analgesic efficacy? Br. J. Pharmacol. *179*, 3592–3611. https://doi.org/10.1111/bph.15327.

34. Storer, R.I., Pike, A., Swain, N.A., Alexandrou, A.J., Bechle, B.M., Blakemore, D.C., Brown, A.D., Castle, N.A., Corbett, M.S., Flanagan, N.J., et al. (2017). Highly potent and selective NaV1.7 inhibitors for use as intravenous agents and chemical probes. Bioorg. Med. Chem. Lett. *27*, 4805–4811. https://doi.org/10.1016/j.bmcl.2017.09.056.

35. Rothenberg, M.E., Tagen, M., Chang, J.H., Boyce-Rustay, J., Friesenhahn, M., Hackos, D.H., Hains, A., Sutherlin, D., Ward, M., and Cho, W. (2019). Safety, tolerability, and pharmacokinetics of GDC-0276, a novel NaV1.7 inhibitor, in a first-in-human, single- and multiple-dose study in healthy volunteers. Clin. Drug Investig. *39*, 873–887. https://doi.org/10.1007/s40261-019-00807-3.

36. Peirs, C., Williams, S.-P.G., Zhao, X., Walsh, C.E., Gedeon, J.Y., Cagle, N.E., Goldring, A.C., Hioki, H., Liu, Z., Marell, P.S., and Seal, R.P. (2015). Dorsal Horn Circuits for Persistent Mechanical Pain. Neuron *87*, 797–812. https://doi.org/10.1016/j.neuron.2015.07.029.

37. Wu, T.D., and Nacu, S. (2010). Fast and SNP-tolerant detection of complex variants and splicing in short reads. Bioinform. Oxf. Engl. *26*, 873–881. https://doi.org/10.1093/bioinformatics/btq057.

38. Pau, G., and Reeder, J. (2023). HTSeqGenie: a NGS Analysis Pipeline. https://bioconductor.org/packages/release/bioc/html/HTSeqGenie.html.

39. Love, M.I., Huber, W., and Anders, S. (2014). Moderated estimation of fold change and dispersion for RNA-seq data with DESeq2. Genome Biol. *15*, 550. https://doi.org/10.1186/s13059-014-0550-8.

40. Ritchie, M.E., Phipson, B., Wu, D., Hu, Y., Law, C.W., Shi, W., and Smyth, G.K. (2015). limma powers differential expression analyses for RNA-sequencing and microarray studies. Nucleic Acids Res. *43*, e47. https://doi.org/10.1093/nar/gkv007.

41. Cong, L., Ran, F.A., Cox, D., Lin, S., Barretto, R., Habib, N., Hsu, P.D., Wu, X., Jiang, W., Marraffini, L.A., et al. (2013). Multiplex genome engineering using CRISPR/Cas systems. Science *339*, 819–823. https://doi.org/10.1126/science.1231143.

42. Mali, P., Yang, L., Esvelt, K.M., Aach, J., Guell, M., DiCarlo, J.E., Norville, J.E., and Church, G.M. (2013). RNA-guided human genome engineering via Cas9. Science *339*, 823–826. https://doi.org/10.1126/science.1232033.

43. Hsu, P.D., Scott, D.A., Weinstein, J.A., Ran, F.A., Konermann, S., Agarwala, V., Li, Y., Fine, E.J., Wu, X., Shalem, O., et al. (2013). DNA targeting specificity of RNA-guided Cas9 nucleases. Nat. Biotechnol. *31*, 827–832. https://doi.org/10.1038/nbt.2647.

44. Sidders, B., Karlsson, A., Kitching, L., Torella, R., Karila, P., and Phelan, A. (2018). Network-based drug discovery: coupling network pharmacology with phenotypic screening for neuronal excitability. J. Mol. Biol. *430*, 3005–3015. https://doi.org/10.1016/j.jmb.2018.07.016.

45. Hargreaves, K., Dubner, R., Brown, F., Flores, C., and Joris, J. (1988). A new and sensitive method for measuring thermal nociception in cutaneous hyperalgesia. Pain *32*, 77–88. https://doi.org/10.1016/0304-3959(88)90026-7.

46. Chaplan, S.R., Bach, F.W., Pogrel, J.W., Chung, J.M., and Yaksh, T.L. (1994). Quantitative assessment of tactile allodynia in the rat paw. J. Neurosci. Methods *53*, 55–63. https://doi.org/10.1016/0165-0270(94)90144-9.

47. Xie, W., Chen, S., Strong, J.A., Li, A.-L., Lewkowich, I.P., and Zhang, J.-M. (2016). Localized sympathectomy reduces mechanical hypersensitivity by restoring normal immune homeostasis in rat models of inflammatory pain. J. Neurosci. *36*, 8712–8725. https://doi.org/10.1523/JNEUROSCI.4118-15.2016.

Please cite this article in press as: Deng et al., Nav1.7 is essential for nociceptor action potentials in the mouse in a manner independent of endogenous opioids, Neuron (2023), https://doi.org/10.1016/j.neuron.2023.05.024

STAR★METHODS

KEY RESOURCES TABLE

REAGENT or RESOURCE	SOURCE	IDENTIFIER
Antibodies		
anti-TH	Millipore	Cat# AB1542; RRID: AB_90755
Anti-Enkephalin	Millipore	Cat# AB1975; RRID: AB_91127
Goat anti-RFP	Rockland	Cat# 200-101-379; RRID:AB_2744552
Rabbit anti-CGRP	Immunostar	Cat# 24112; RRID:AB_572217
Mouse anti-NF200	Sigma	Cat# N0142; RRID:AB_477257
Rabbit anti-TH	Millipore Sigma	Cat# AB152; RRID:AB_390204
Chemicals, peptides, and recombinant proteins		
GNE-3565	Genentech	N/A
Naloxone	Tocris	1453005
Morphine	Sigma	M-005
Phenylephrine HCl	Sigma	P6126
AITC	Sigma	377430
Isolectin GS-IB4 From Griffonia simplicifolia, Alexa Fluor™ 647 Conjugate	Invitrogen	I32450
NeuroTrace™ 435/455 Blue Fluorescent Nissl Stain	Invitrogen	N21479
Critical commercial assays		
Nav1.7 Taqman assay	Custom design; Shields et al.[25]	N/A
TH Taqman assay	ThermoFisher Scientific	Mm00447557_m1
PENK Taqman assay	ThermoFisher Scientific	Mm01212875_m1
Ceacam10 Taqman assay	ThermoFisher Scientific	Mm00483250_m1
Deposited data		
Bulk and single cell RNAseq	This study	GEO accession number GEO: GSE213827
Experimental models: Organisms/strains		
Mouse: Nav1.7 flox; ERT cre	Shields et al.[25]	N/A
Mouse: Nav1.7 flox; vGlut3 cre	Cre line from Peirs et al., *Neuron* 2015[36]	N/A
Mouse: YWV->SRL Nav1.7	This manuscript	N/A
Mouse: YW->SR Nav1.6	This manuscript	N/A
Oligonucleotides		
RNAscope Probe Mm-Penk-C2	ACDInc	318768-C2
RNAscope Probe Nav1.7	ACDInc	457648 Mm-Scn9a-01
Recombinant DNA		
pBi_hNav1.7/hBeta2	Ahuja et al.[28]	N/A
Software and algorithms		
Prism (v9.4)	GraphPad software	www.graphpad.com
Spike2	Cambridge Electronic Design	www.ced.co.uk
pCLAMP11	Molecular Devices	www.moleculardevices.com
Origin	OriginLab	www.originlab.com
FIJI/ImageJ	Fiji/NIH	www.fiji.sc
GSNAP alignment tool	Wu and Nacu[37]	http://research-pub.gene.com/gmap/

(*Continued on next page*)

Continued

REAGENT or RESOURCE	SOURCE	IDENTIFIER
HTSeqGenie (Bioconductor)	Pau and Reeder[38]	https://bioconductor.org/packages/release/bioc/html/HTSeqGenie.html
DESeq2 (Bioconductor)	Love et al.[39]	https://bioconductor.org/packages/release/bioc/html/DESeq2.html
limma (Bioconductor)	Ritchie et al.[40]	http://bioconductor.org/packages/release/bioc/html/limma.html
Cellranger (v3.1.0)	10x Genomics	www.10xgenomics.com
Cellbender (v0.2.0)	Broad Institute	https://cellbender.readthedocs.io/en/latest/index.html
Seurat (v3.1.1)	Satija Lab	https://satijalab.org/seurat/

RESOURCE AVAILABILITY

Lead contact

Further information and requests for resources and reagents should be directed to and will be fulfilled by the lead contact, David Hackos (hackos.david@gene.com).

Materials availability

The compound GNE-3565 is available by the lead contact upon request. Synthesis is described at the end of the STAR Methods section. The Nav1.7 MBS mouse is also available by the lead contact upon request.

Data and code availability

- Datasets have been deposited in the Gene Expression Omnibus (GEO) repository, accession number GEO: GSE213827 (https://www.ncbi.nlm.nih.gov/geo/query/acc.cgi?acc=GSE213827).
- No original code was used in the analysis of these results.
- Any additional information required to reanalyze the data reported in this work paper is available from the lead contact upon request.

EXPERIMENTAL MODEL AND STUDY PARTICIPANT DETAILS

Mouse and mouse lines

All animal experiments were approved by the Institutional Animal Care and Use Committee of Genentech. The following mouse lines have been used in this study: Nav1.7 fl/fl; ERT.cre, Nav1.7 fl/fl; vGLUT3.cre, YW->SR NaV1.6 KI and YWV->SRL Nav1.7 KI. Nav1.7 fl/fl; ERT.cre mice were generated by crossing Nav1.7 fl/fl Ert.cre.pos X Nav1.7 fl/fl; ERT.cre.neg yielding 50% cre.pos mice and 50% cre.neg mice. Nav1.7 fl/fl; vGLUT3 mice were bred using a similar strategy. Mice were housed on a 12:12 hour light-dark cycle with food and water available ad libitum and only healthy mice were used for experiments. Genotyping was done using genomic DNA isolated from tail clip biopsies for PCR. Both male and female mice were used in experiments with age ranging from 8 weeks to 16 weeks. No statistically-significant differences in experimental results between male and female mice were observed in our studies. All mouse experiments were performed blinded and randomization was done to ensure that tested mice started at the same average baseline. All drug treated mice were drug-naïve at the beginning of the experiment. Behavioral experiments were conducted in two (or more) separate cohorts, with the data combined in the final analysis. No significant differences were observed between cohorts in any experiment.

Generation of SCN9A YWV→SRL KI mouse

CRISPR/Cas9 technology[41,42] was used to generate a genetically modified mouse strain with a *Scn9a* YWV2SRL knockin. A single guide RNA (sgRNA) target and protospacer adjacent motifs (PAM) were identified in *Scn9a* ENSMUSG00000075316 genomic region of interest using the CRISPR design tool (Benchling) that uses an algorithm[43] to provide 'MIT' specificity scores for each sgRNA, as well as the top 15 predicted off-target loci and corresponding MIT off-target scores. The guide target was: 5' TGTGC TATACTGGATCAACG 3'; PAM: TGG with an algorithm score of 65.8. Predicted cut sites are between 66317841-66317842 genome coordinates. An oligonucleotide donor

5'GTTCTTATCTGCCTCAATATGGTAACCATGATGGTAGAAAAAGAGGGGCAAACTGACTACATGAGTTTTGTGCTAtcacggAT CAAtctgGTCTTCATCATCCTGTTCACTGGGGAGTGTGTGCTGAAGCTGATCTCTCTCAGGCATTACTACTTCACTGTGGGAT 3'

The first point mutation of Y1546S (TAC–>TCA) is located at 66,317,851-66,317,849 genome coordinates, and a second point mutation of W1547R (TGG–>CGG) is located at 66,317,848-66,317,846 genome coordinates, and the third point mutation of V1550L

(GTG–>CTG) is located at 66,317,839-66,317,837. A silent mutation was created at the beginning of the gRNA to prevent Cas9 from cutting the donor oligo. The silent mutation of AAC>AAT is located at 66,317,842-66,317,840 genome coordinates. After homology-directed repair of Cas9-induced chromosome breaks with the oligonucleotide donor, the YWV2SRL protein will be expressed. Once a sgRNA decision was finalized, the off-target list was used to identify the top 15, and next-generation sequencing (NGS) amplicon primers were designed for the on-target locus, and each of the off-targets synthetic guide RNA was obtained from Synthego. CAS9 protein was obtained from PROTEIN SOURCE and complexed with sgRNA before microinjection. Reagent concentrations for microinjection were as follows: 25 ng/μl Cas9 mRNA (Thermo Fisher; A29378) + 13 ng/μl sgRNA (Synthego), Oligonucleotide donor (50 ng/ul) (IDT). After zygote microinjection and embryo transfer, genomic DNA was prepared from tail tip biopsies of potential G0 founders and G0 animals were first analyzed by droplet digital PCR (Bio-Rad). Primers were used to amplify the HDR event (ON Target) and the 15 most likely off-target sites. Only G0 mosaic founders positive for the intended mutation were screened by targeted amplicon NGS. Amplicons were submitted for NGS analysis.

Founders were selected for mating with wild-type C57BL/6N mice for germline transmission of the gene edited chromosome. Subsequent analysis of genomic DNA from G1 pups was used to confirm germline transmission of the targeted gene and the absence of off-target hits elsewhere in the genome.

Generation of SCN8A YW→SR KI mouse

CRISPR/Cas9 technology[41,42] was used to generate a genetically modified mouse strain with a SCN8A YW2SR knockin. A single guide RNA (sgRNA) target and protospacer adjacent motifs (PAM) were identified in Scn8a ENSMUSG00000023033 genomic region of interest using the CRISPR design tool (Benchling) that uses an algorithm[43] to provide 'MIT' specificity scores for each sgRNA, as well as the top 15 predicted off-target loci and corresponding MIT off-target scores.

The guide target was: 5' CATTCTCTACTGGATTAATC 3'; PAM: TGG with an algorithm score of 42.3. Predicted cut sites are between 100,933,463-100,933,464 genome coordinates. An oligonucleotide donor

5'ATGCTTATCTGCCTTAACATGGTGACCATGATGGTGGAGACAGACACACAGAGCAAGCAGATGGAGAACATTCTCTctcGGATTAATCTGGTCTTCGTCATCTTCTTCACCTGCGAGTGTGTGCTCAAAATGTTTGCCTTGAGACACTACTATTTC 3'

The first point mutation of PM: Y1553S (TAC–>TCT) is located at 100,933,454-100,933,456 genome coordinates, and a second point mutation of PM: W1554R (TGG–>CGG)is located at 100,933,457 100,933,459 genome coordinates. After homology-directed repair of Cas9-induced chromosome breaks with the oligonucleotide donor, the YW2SR protein will be expressed. Once a sgRNA decision was finalized, the off-target list was used to identify the top 15, and next-generation sequencing (NGS) amplicon primers were designed for the on-target locus, and each of the off-targets synthetic guide RNA was obtained from Synthego. CAS9 protein was obtained from PROTEIN SOURCE and complexed with sgRNA before microinjection. Reagent concentrations for microinjection were as follows: 25 ng/μl Cas9 mRNA (Thermo Fisher; A29378) + 13 ng/μl sgRNA (Synthego), Oligonucleotide donor (50 ng/ul) (IDT).

After zygote microinjection and embryo transfer, genomic DNA was prepared from tail tip biopsies of potential G0 founders, and G0 animals were first analyzed by droplet digital PCR (Bio-Rad). Primers were used to amplify the HDR event (ON Target) and the 15 most likely off-target sites. Only G0 mosaic founders positive for the intended mutation were screened by targeted amplicon NGS. Amplicons were submitted for NGS analysis.

Founders were selected for mating with wild-type C57BL/6N mice for germline transmission of the gene edited chromosome. Subsequent analysis of genomic DNA from G1 pups was used to confirm germline transmission of the targeted gene and the absence of off-target hits elsewhere in the genome.

METHOD DETAILS

Quantitative PCR (qPCR)

Quantitative PCR (qPCR) were performed as described previously.[25] Briefly, DRG, TG and SCG were firstly collected from either Nav1.7 cKO mice (ERT.cre+; SCN9a.loxP) and littermate controls (ERT.cre-; SCN9a.loxP) at indicated time points following tamoxifen i.p. dosing or WT mice 1 hour after P.O. dosing with vehicle or 30 mg/kg G03253565. Secondly, total RNA was purified and then reverse transcribed into complementary DNA using a QIAGEN RNAeasy Lipid Tissue kit (#74804) and an Ambion Cells-to-Ct kit (AM1728), respectively. Lastly, qPCR was performed in an ABI viiA7 system (Applied Biosystems). To confirm tamoxifen induced Nav1.7 KO, a custom-designed TaqMan assay was used which detects expression of a *Scn9a* gene sequence crossing the boundary of exons 16 and 17. The other TaqMan assays were obtained from Thermo Fisher Scientific. Gene expression difference was quantified as either relative expression to the internal β-actin control (delta Ct) or normalized expression to the levels of control littermates.

Dynaflow patch clamp recording

Compound Kd and IC50 were measured using a Cellectricon Dynaflow (Cellectricon) all-glass perfusion system, which allows rapid solution exchange and prevents stickiness issues that occur with plastic perfusion systems. Compound solutions were loaded in the 16 wells of a dynaflow chip and the human Nav isoform stably expressing HEK293 cells were lifted using patch pipettes and positioned in front of the micro-channel outlets. The patch pipettes had tip resistances of 3-5 MΩ and were back filled with intracellular solution containing (in mM): 140 CsF, 10 NaCl, 1.5 $MgCl_2$, 5 EGTA, 10 HEPES, pH of 7.4 and osmolality of 300 mOsm. The Nav stably expressing HEK293 cells were continuously perfused with extracellular solution containing (in mM): 140 NaCl, 2 KCl, 1 $MgCl_2$,

1 $CaCl_2$, 10 HEPES, pH of 7.4 and osmolality of 310 mOsm. Whole-cell recordings were obtained using an Axopatch 200B amplifier, filtered at 1 Hz and sampled at 10 Hz. Because the tool compound GNE-3565 is a state dependent blocker that only binds to the inactivated state of Nav channels, the membrane holding potential for a particular Nav isoform was adjusted to a level where ~90% of channels were inactivated. As a consequence, the holding potentials were -60 mV for Nav1.5 and 1.7 and -40 mV for Nav1.1, 1.2, 1.3, 1.4, and 1.6, respectively. All recordings were performed at room temperature. K_d was calculated using kinetics measurement as previously described. Briefly, K_{obs} and K_{off} were measured using single exponential fits of compound association and disassociation kinetics. Kon was then calculated using the equation as $K_{obs} = K_{on} \times [conc] + K_{off}$ and K_d was calculated using equation $K_d = K_{off} / K_{on}$. Compound IC50s were calculated by fitting dose-response curves with a standard Hill function. Results are the average of 3-5 independent measurements and are expressed as mean ± SEM.

In vitro field stimulation and calcium imaging

Compound IC50 was determined using an Optical Electrophysiology Platform (Cellectricon).[44] DRGs from adult mice were microsurgically dissected and plated in Neurobasal A medium with B27 with 10 ng NGF/ml into 48 wells in Cellaxess Elektra laminin-coated, poly-D-Lysine coated 384-well plates (CHX300105, Cellectricon) and thereafter incubated at 37 °C, 5% CO_2. Electric filed stimulation (EFS) experiments were performed approximately 72 hours post plating. At the day of the experiment, Component A (FLIPR Calcium 5 Assay Kit (Molecular Devices #R8185) and Compound were added to the wells 1h prior to EFS. Compound was tested in six concentrations (in duplicate per plate at two independent test occasions). In addition to above, wells with max effect controls (tetracaine, 30 μM) and min effect controls (wells with medium and normalized [DMSO]) were included for normalization purposes. The plates were inserted into Cellectricon's Optical Electrophysiology Platform and EFS was evoked. Simultaneously, images were acquired to enable quantification of EFS-evoked calcium influx. The temperature in the instrument was kept at 22–25 °C during the experiment. The calcium response was analyzed by dividing the peak response of the EFS-evoked calcium influx with the baseline immediately preceding the EFS. Compound IC50 was calculated from the normalized values by fitting dose-response curves with a standard Hill function. Results are the average of two wells per experiment from 2 independent experiments and are expressed as mean ± SEM.

In vivo electrophysiological recording

Blood pressure monitoring

Animal preparation. The procedure is performed under isoflurane anaesthesia (5% for induction followed by 2.5% maintenance, using a yearly serviced Penlon Sigma Delta vaporiser). Induction of anaesthesia is achieved in a perspex box. Once the level of anaesthesia is sufficient and respiratory frequency visibly reduced, the animal is transferred to the operating table and fitted on a nose cone. Body temperature, measured with a rectal probe, is maintained at 37±0.5 °C using a feedback-controlled heating blanket (Harvard Apparatus, model 50-7061). Adequate depth of anaesthesia is checked by lack of withdrawal reflex to severe pinch of the paw.

The carotid artery and jugular vein are then catheterised (stretched 18G Portex Intravenous Cannula, approximately 0.3 mm external diameter) for blood pressure recording and i.v. injection, respectively. A tracheotomy is performed and a Y connector is secured in the trachea. The animal is connected to a rodent ventilator (CWE Inc., model SAR-1000). Isoflurane, previously provided through the nose cone, is now provided through artificial ventilation. Artificial ventilation is maintained throughout the experiment using a positive pressure, inspired volume-controlled approach (1/3 inspiration/expiration ratio, 95-105 breaths/min, 14 μl/μg tidal volume) using a 1/4 O2/air mixture.

Experimental protocol. The compound is injected i.v. over 10 min (T0 to T10), 10 min after completion of the surgical preparation. Cardiovascular parameters are further monitored for 5 min after completion of the compound injection. Blood sampling is performed to control blood gas and pH using a GemPremier3000 (Werfen Instrumentation Laboratory), and to generate plasma samples to determine compound exposure. The animal is culled with an overdose of pentobarbital.

Quantifications of responses. Blood pressure and heart rate are measured and averaged in 1 min bin from 5 min before to 15 min after the start of the compound injection.

Data acquisition set up. The blood pressure catheter (filled with heparinized saline, 50 IU/ml) is connected to a pressure transducer (DTX Plus, Becton Dickinson). Analog signal from the pressure transducer is amplified with a NL108 amplifier (Digitimer) and digitized at 100 Hz/

Data acquisition data data quantification are achieved with a Power 1401 mark II (Cambridge Electronic Design) driven by a PC using Spike 2 software, version 7.09.

Dorsal root ganglia recording

Animal preparation. The procedure is performed under isoflurane anesthesia (5% for induction followed by 2.5% maintenance, using a yearly serviced Penlon Sigma Delta vaporizer). Induction of anesthesia is achieved in a perspex box. Once the level of anesthesia is sufficient and respiratory frequency visibly reduced, the animal is transferred to the operating table and fitted on a nose cone. Body temperature, measured with a rectal probe, is maintained at 37±0.5 °C using a feedback-controlled heating blanket (Harvard Apparatus, model 50-7061). Adequate depth of anesthesia is checked by lack of withdrawal reflex to severe pinch of the paw.

The carotid artery and jugular vein are then catheterized (stretched 18G Portex Intravenous Cannula, approximately 0.3 mm external diameter) for blood pressure recording and i.v. injection, respectively. A tracheotomy is performed and a Y connector is secured in the trachea. The animal is connected to a rodent ventilator (CWE Inc., model SAR-1000). Isoflurane, previously provided through the nose cone, is now provided through artificial ventilation. Artificial ventilation is maintained throughout the experiment

using a positive pressure, inspired volume-controlled approach (1/3 inspiration/expiration ratio, 95-105 breaths/min, 14 μl/μg tidal volume) using a 1/4 O2/air mixture.

The animal is placed in a stereotaxic frame. The skin of the back is shaved. The lateral aspects of the L4 vertebra are exposed after a dorsal midline incision. The rostral part of the L4 vertebrae is clamped with spinal forks and a medio-lateral laminectomy is performed to uncover the left L4 DRG. Two needles connected to a current generator are then inserted s.c. on each side of the paw.

Once the animal preparation is completed, isoflurane is reduced to 1.8 %. During the recording, spontaneous breathing movements, which interfere with electrophysiological recording, are minimized by paralyzing the animal with D-tubocurarine. Metabolic acidosis and hypoglycemia are compensated by supplying sodium bicarbonate and glucose as an intravenous infusion of 2 μl/g/h of a solution containing 50 mg/ml glucose, 55 mg/ml $NaHCO_3$ and 200 μg/ml D-tubocurarine in distilled water. Blood pressure decrease due to blood loss is compensated, when necessary, by the i.v. delivery of Hemopure® (glutaraldehyde cross-linked bovine hemoglobin polymers, which range in size from 130 to 500 kDa and have an average molecular weight of 250 kDa). The maximal volume of Hemopure® delivered during an experiment is 100 μl.

Experimental protocol

Search of neurons. Neurons are searched for using electrical stimulations of the hind paw (square wave pulses, 10 mA, 2 ms, at 1 Hz). The neuron is considered ad hoc for the experiment if the latency of the electrically generated action potential is $\geq$25 ms and if the signal to noise ratio is sufficient to allow unambiguous quantification of the evoked responses.

Initial characterization. The receptive field is determined by exerting light pinches with hand held forceps, or moving an ice chip across the paw, or by repositioning the stimulating needles until the space between them corresponds to 2 digits or less.

Responses of the neuron to a range of mechanical and thermal stimuli are then evoked (initial characterization). Mechanical stimuli consist of the serial application of 10 strokes with hog brush, application of home-made Von Frey hair exerting a force of 25, 50, 100 and 200 mN over a tip of 1.1 mm diameter (i.e. 3.8 mm^2), and pinch with mini hemostat clamp (reference 18055-01 Fine Science Tools). An identical Von Frey hair exerting a force of 500 mN is used instead of pinch when the receptive field is not amenable to pinch (e.g. center of the palm of the paw). Mechanical stimuli are applied for 6 s. Thermal stimuli consist of application of 10 ml of water at 0, 24, 42, 46 and 50 °C, flowing by gravity from a 25 ml Pipette and targeting the entire receptive field (duration of the flow is approximately 3 s).

Drug testing. The stimulating needles are positioned to allow the application of mechanical or thermal stimuli while allowing the generation of electrically induced action potential. The ad hoc stimuli are chosen (WJ at 0 °C, or 50 °C, or VF200mN or pinch, for cold, heat and mechanical specific nociceptors, respectively; VF200mN or pinch, or WJ at 50°C for polymodal nociceptors).

Electrical stimulations (1 pulse every 6 s) are now applied throughout the experiment but during the application of the "natural" noxious stimulus previously chosen. Once the action potential reaches a stable value, the noxious stimulus is applied (Time 0, T0) and the compound is injected i.v. over 10 min (completion of injection at T0+10 min, T10). Electrical stimulations are continued for 5 min after completion of the i.v. injection. The noxious stimulus is applied again.

Once the injection of compound has started, boluses of phenylephrine (1 mg/ml in Ringer lactate; 0.15 μl volume) are injected using a 100 μl Hamilton syringe connected to the jugular vein in order to limit the drop in blood pressure induced by the compound. The Hamilton syringe is fitted in a KD Scientific model 200 syringe pump which is switched on/off to deliver the bolus over 1.5 s every time the diastolic blood pressure falls below a pre-set value. On/off switches are driven by TTL output from the power 1401 mark 2 using built-in commands from the output sequencer based on blood pressure channel measures. The instruction is iterated with each electrical stimulation, i.e. every 6 s. The pre-set value (50, 60 or 70 mmHg) is set to approximately match the value of diastolic blood pressure minus 10 mmHg at the onset of compound injection.

Blood sampling. Blood sampling is performed to control blood gas and pH using a GemPremier3000 (Werfen Instrumentation Laboratory), and to generate plasma samples to determine compound exposure. The animal is culled with an overdose of pentobarbital.

Quantifications of responses. Evoked responses are quantified as number of action potentials. Responses to mechanical stimuli are quantified for 5 s. Responses to thermal stimuli are quantified for their entire duration (from 3 to 30 s).

For electrically induced responses, the latency of the action potential and the intensity of the electrical stimulation are measured throughout the experiment.

Blood pressure is measured and averaged for 1 min at T0, T5, T10 and T15.

Data acquisition set up. The blood pressure catheter (filled with heparinized saline, 50 IU/ml) is connected to a pressure transducer (DTX Plus, Becton Dickinson). Analog signal from the pressure transducer is amplified with a NL108 amplifier (Digitimer). A tungsten-in-glass microelectrode (2 MΩ impedance, fine tip, 125 μm shaft diameter, Kation Scientific) connected to a head stage (NL104, Digitimer) is used for recording of electrical activity. Reference and second active source from the headstage are shunted by a jumper to the same flying lead connected to the preparation. Analog signal from the headstage is amplified (x20 k gain, NL104A, Digitimer) and filtered (2-3 kHz band pass, NL125/126, Digitimer, plus 50 Hz cancellation, Hum Bug, Quest scientific). Electrical stimulations are delivered with an A365 stimulus isolator (World Precision Instrument). Analog signals are digitized at 30 KHz for spinal cord extracellular electrical activity and 100 Hz for blood pressure.

Data acquisition, data quantification and overall control of the experiments (notably the timing of electrical stimulations and on/off switch of pump for blood pressure control) are achieved with a Power 1401 mark II (Cambridge Electronic Design) driven by a PC using Spike 2 software, version 7.09.

Spinal cord neuron recording

Animal preparation. The procedure is performed under isoflurane anesthesia (5% for induction followed by 2.5% maintenance, using a yearly serviced Penlon Sigma Delta vaporizer). Induction of anesthesia is achieved in a perspex box. Once the level of anesthesia is sufficient and respiratory frequency visibly reduced, the animal is transferred to the operating table and fitted on a nose cone. Body temperature, measured with a rectal probe, is maintained at 37±0.5 °C using a feedback-controlled heating blanket (Harvard Apparatus, model 50-7061). Adequate depth of anesthesia is checked by lack of withdrawal reflex to severe pinch of the paw.

The carotid artery and jugular vein are then catheterized (stretched 18G Portex Intravenous Cannula, approximately 0.3 mm external diameter) for blood pressure recording and i.v. injection, respectively. A tracheotomy is performed and a Y connector is secured in the trachea. The animal is connected to a rodent ventilator (CWE Inc., model SAR-1000). Isoflurane, previously provided through the nose cone, is now provided through artificial ventilation. Artificial ventilation is maintained throughout the experiment using a positive pressure, inspired volume-controlled approach (1/3 inspiration/expiration ratio, 95-105 breaths/min, 14 μl/μg tidal volume) using a 1/4 O2/air mixture.

The animal is placed in a stereotaxic frame. The skin of the back is shaved with an electric shaver. The lateral aspect of the T12-L2 vertebrae is exposed after a dorsal midline incision. The T12-L2 vertebrae are clamped with spinal forks and a laminectomy of the L1 vertebra is performed to uncover the lumbosacral enlargement. The dura is cut using a 21 G needle as a micro-blade and retracted with fine forceps. A well is made with agarose gel (2% in 9 g/l NaCl in distilled water) around the lumbosacral laminectomy. The well is filled with mineral oil.

Once the animal preparation is completed, isoflurane is reduced to 1.8 %. During the recording, spontaneous breathing movements, which interfere with electrophysiological recording, are minimized by paralyzing the animal with D-tubocurarine. Metabolic acidosis and hypoglycemia are compensated by supplying sodium bicarbonate and glucose as an intravenous infusion of 2 μl/g/h of a solution containing 50 mg/ml glucose, 55 mg/ml $NaHCO_3$ and 200 μg/ml D-tubocurarine in distilled water. Blood pressure decrease due to blood loss is compensated, when necessary, by the i.v. delivery of Hemopure® (glutaraldehyde cross-linked bovine hemoglobin polymers, which range in size from 130 to 500 kDa and have an average molecular weight of 250 kDa). The maximal volume of Hemopure® delivered during an experiment is 100 μl.

Experimental protocol

Search of neurons. Neurons are searched for using gentle tapping of the hind paw with one finger. A neuron is considered ad hoc for the experiment if it displays a sustained response to light pinch with hand held forceps, and a marked response to a 5 ml water jet test at 50 °C (polymodal neuron). The receptive field is then delineated with light pinches with hand held forceps. The most sensitive site of the receptive field is used for the subsequent mechanical and thermal stimulations. A pair of 30 G needles connected to an electrical stimulator are then inserted on the edge of the receptive field to allow electrical stimulations and mechanical and thermal stimulations.

Initial characterization and drug testing. Responses of the neuron to a range of mechanical and thermal stimuli are then evoked. Mechanical stimuli consist of the serial application of 10 strokes with camel and hog brushes, application of home-made Von Frey hair exerting a force of 25, 50, 100 and 200 mN over a tip of 1.1 mm diameter (i.e. 3.8 mm^2), and pinch with mini hemostat clamp (reference 18055-01 from Fine Science Tools). Mechanical stimuli are applied for 6 s. Thermal stimuli consist of application of 10 ml of water at 0 °C, room temperature (RT, 23-24 °C), 42 °C, 46 °C and 50 °C, flowing by gravity from a 25 ml Pipette and targeting the entire receptive field (duration of the flow is approximately 3 s).

The intensity of the electrical stimulation is set to obtain 10-15 C fibre related action potential (test intensity) using square wave pulses of 2 ms duration, 1-10 mA. Electrical stimulations are delivered every 15 s. Once the number of C-fibre related action potential reaches a stable value, the compound is injected i.v. over 10 min (T0 to T10). Electrical stimulations are continued for 5 min after completion of the i.v. injection. The series of mechanical and thermal stimuli initially used is then applied.

Once the injection of compound has started, boluses of phenylephrine (1 mg/ml in Ringer lactate; 0.15 μl volume) are injected using a 100 μl Hamilton syringe connected to the jugular vein in order to limit the drop in blood pressure induced by the compound. The Hamilton syringe is fitted in a KD Scientific model 200 syringe pump which is switched on/off to deliver the bolus over 1.5 s every time the diastolic blood pressure falls below a pre-set value. On/off switches are driven by TTL output from the power 1401 mark 2 using built-in commands from the output sequencer based on blood pressure channel measures. The instruction is iterated with each electrical stimulation, i.e. every 15 s. The pre-set value (50, 60 or 70 mmHg) is set to approximately match the value of diastolic blood pressure minus 10 mmHg at the onset of compound injection.

Blood sampling. Blood sampling is performed to control blood gas and pH using a GemPremier3000 (Werfen Instrumentation Laboratory), and to generate plasma samples to determine compound exposure. The animal is culled with an overdose of pentobarbital.

Quantifications of responses. Evoked responses are quantified as number of action potentials. Responses to mechanical stimuli are quantified for 5 s. Responses to thermal stimuli are quantified for their entire duration (from 3 to 30 s).

For electrically induced responses, the number of C fibre related action potentials is measured throughout the experiment. The mean latency is measured at T0, T3, T6, T9, T12 and T15. Blood pressure is measured and averaged for 1 min at T0, T5, T10 and T15.

Data acquisition set up. The blood pressure catheter (filled with heparinized saline, 50 IU/ml) is connected to a pressure transducer (DTX Plus, Becton Dickinson). Analog signal from the pressure transducer is amplified with a NL108 amplifier (Digitimer). A tungsten-in-glass microelectrode (2 MΩ impedance, fine tip, 125 μm shaft diameter, Kation Scientific) connected to a head stage (NL104, Digitimer) is used for recording of electrical activity. Reference and second active source from the headstage are shunted by a jumper to

the same flying lead connected to the preparation. Analog signal from the headstage is amplified (x20 k gain, NL104A, Digitimer) and filtered (2-3 kHz band pass, NL125/126, Digitimer, plus 50 Hz cancellation, Hum Bug, Quest scientific). Electrical stimulations are delivered with an A365 stimulus isolator (World Precision Instrument). Analog signals are digitized at 30 KHz for spinal cord extracellular electrical activity and 100 Hz for blood pressure.

Data acquisition, data quantification and overall control of the experiments (notably the timing of electrical stimulations and on/off switch of pump for blood pressure control) are achieved with a Power 1401 mark II (Cambridge Electronic Design) driven by a PC using Spike 2 software, version 7.09.

Bulk RNAseq

Mice at 12-18 weeks of age were used for the bulk RNAseq study. No sex-specific differences were observed in the sequencing results. Six weeks after tamoxifen intraperitoneal injection (3 injections of 100 mg/kg separated by 24 h; 10 ml/kg in corn oil), DRGs from cKO and control animals were isolated and total RNA was purified using a RNeasy-Lipid Tissue Kit (7400, Qiagen). DRGs were isolated from 12 mice (6 Nav1.7 cre.pos and 6 Nav1.7 cre.neg mice mixed sex). RNA samples passing a mRNA quality check were proceeded to quantitative analysis on an Illumina Hiseq 2000. The fastq sequence files for all RNA-seq samples were filtered for read quality and ribosomal RNA contamination. The remaining reads were then aligned to the mouse reference genome (GRCn38) using the GSNAP alignment tool.[37] Alignments were produced using the following GSNAP parameters: '-M 2 n 10 -B 2 -i 1 N 1 w 200000 -E 1 –pairmax-rna = 200000 –clip-overlap'. These steps, and the downstream processing of the resulting alignments to obtain read counts and normalized Reads Per Kilobase Million (nRPKMs) per gene (over all exons of RefSeq gene models), are implemented in the Bioconductor package, HTSeqGenie.[38] Only uniquely mapped reads were used for further analysis. Read counts were adjusted based on DESeq2 estimated sizeFactor[39] and weighted by their mean-variance relationship as estimated by voom. Differential gene expression was performed using the limma empirical Bayes analysis pipeline described in the R package limma.[40] A prefilter was applied on the read counts such that only genes with at least ten counts in at least three samples (of any condition) were analyzed. P-values for other genes were simply set to 1 and log-fold-changes to 0 for visualization purposes, but such genes were not included in the multiple testing correction. Histogram analysis was performed by analyzing expression of genes selectively expressed in specific populations of DRG neurons as previously defined[26] (cLTMRs (th), neurofilament positive (NF+) myelinated neurons (nf1, nf2, nf3, nf4, and nf5), non-peptidergic (NP) nociceptors (np1, np2, np3), and peptidergic (Pep) nociceptors (pep1, pep2)).

Single cell RNAseq

Four weeks after Tamoxifen injections, mice were euthanized by CO2 inhalation and DRGs were excised bilaterally for dissociation and subsequent RNA extraction or single cell library preparation and sequencing. For these studies, samples were paired, Cre+ and Cre- for each run. Lumbar DRGs L4, L5,L6 for each animal excised and enzymatically dissociated with collagenase/Trypsin. DRGs (6 DRGs per mouse) from 12 mice (7 Nav1.7 cre.pos and 5 Nav1.7 cre.neg mice mixed sex) and from 4 vglut3.cre mice (2 Nav1.7 cre.pos and 2 Nav1.7 cre.neg). We chopped the DRGs and enzymatically digested them using a combination of collagenase and trypsin with gentle shaking. DRG cells were then dissociated by gentle trituration using 1 mL and 200 mL pipet tips. The cell suspensions were purified by myelin elimination using magnetic anti-myelin beads and suspended in HibernateA containing 10% inactivated horse serum.

Viable cells were counted on a BioRad automated cell counter, using Calcein-AM labeling (PromoKine). Cells were washed 3X and suspended in Hibernate A medium containing 10% inactivated horse serum, 0.2 U/uL RNase inhibitor for single cell capture and transcript library generation using the 10X Genomics sequencing platform. Libraries were generated using a 3' expression library prep kit (10X Genomics) and sequenced on an Illumina Hiseq instrument.

Single nuclei sequencing

Data processing

Raw sequencing reads were processed and aligned to the mouse reference transcriptome (GRCm38) via the 10x software Cellranger (v3.1.0) using default parameters to generate the raw feature and barcodes matrices. CellBender (v0.2.0) was used to remove ambient RNA effects from raw gene-by-cell count matrices for each sample using the remove-background function with the following parameters: epochs=200, fpr=0.01, total-droplets-included=30000, and expected-cells=number of cells called by CellRanger. CellBender produces processed and filtered gene-by-cell count matrices corrected for ambient RNA.

Individual samples were merged and analyzed using Seurat (v3.1.1) following the standard workflow. Briefly, cells with less than 500 UMIs or mitochondria RNA content greater than 25% were filtered. For each cell, the feature expression counts were normalized by the total expression and log transformed. Next, feature selection was determined by computing the top 1000 highly variable genes using the vst method. Finally, count values per gene was zero center scaled prior to dimension reduction analysis.

Single cell cluster analysis

Principal component analysis was performed on scaled data and the top 30 components were used for UMAP analysis. Clusters were identified by first constructing a KNN graph based on the euclidean distance in of the top 30 components in PCA space, then using a Louvain algorithm to iteratively group cells together. A range of resolution parameters were used in the FindClusters function and the best resolution was visually determined based on marker expression and known biology.

Please cite this article in press as: Deng et al., Nav1.7 is essential for nociceptor action potentials in the mouse in a manner independent of endogenous opioids, Neuron (2023), https://doi.org/10.1016/j.neuron.2023.05.024

Immunohistochemistry

For examination of tdTomato expression across DRG neuronal populations in vGluT3.Cre.tdT mice, lumbar DRGs were collected from male and female adult mice and drop-fixed in 4% paraformaldehyde (PFA) for 2 hours at room temperature. For Nav1.7 KO induced enkephalin expression, lumbar spinal cords were dissected out from Nav1.7 cKO and littermate WT mice following 4% PFA perfusion. The spinal cord sections were further post-fixed in 4% PFA overnight at 4°C. DRGs and spinal cords were then washed in PBS, transferred to 30% sucrose at 4°C for 2-3 days, rapidly frozen in Tissue-Tek O.C.T. Compound, sectioned at 14μm onto Superfrost Plus slides, and stored at -80oC until staining.

Prior to immunostaining, sections were dried at room temperature for 30 min, washed with PBS, and a hydrophobic barrier was drawn using an ImmEdge PAP Pen. Sections were incubated for 1 hour at room temperature with blocking buffer (10% Normal Donkey Serum + 0.3% Triton X-100 in PBS). Primary antibodies mixtures were prepared in blocking buffer and sections were incubated overnight at 4°C. The following primary antibodies have been used in this study: goat anti-RFP (1:1000, Rockland #200-101-379), mouse anti-NF200 (1:500, Sigma N0142), rabbit anti-CGRP (1:1000, Immunostar, 24112), rabbit anti-TH (1:1000, Millipore Sigma AB152), or rabbit anti-Enkephalin, Met antibody (1:2000, Millipore, AB1975). Sections were washed with PBS + 0.1% Triton X-100 and then incubated with Cy3-donkey anti-goat (1:500, Jackson ImmunoResearch 705-165-147) in combination with IB4-AlexaFluor647 (1:500, Invitrogen I32450) or appropriate secondary antibodies (1:500 Alexa647-donkey anti-IgG, Jackson ImmunoResearch) in blocking buffer at room temperature for 2 hours. Sections were washed with PBS + 0.1% Triton X-100 and counterstained with NeuroTrace 435/455 Blue Fluorescent Nissl Stain (1:100 in PBS, Invitrogen N21479) at room temperature for 1 hour before being coverslipped with ProLong Gold (Invitrogen P36930).

For DRG staining, epifluorescence images were taken using a Zeiss Axio Imager.M2 upright microscope equipped with an Apotome.2 structured illumination module. Images were acquired using a Zeiss Colibri 7 LED, DAPI/AF555/Cy5 filter sets, a Plan-Apochromat 20X/0.8 objective lens, and a Hamamatsu ORCA-Flash 4.0 Digital CMOS camera. A single Z-plane was imaged per DRG, with 2-3 DRGs imaged per animal, and the resulting images were stitched and Apotome-processed with Zeiss Zen software. Images were analyzed using custom macros in FIJI/ImageJ. Neuronal regions-of-interest were segmented automatically using Cellpose (https://www.nature.com/articles/s41592-020-01018-x) on the Nissl channel and manually confirmed or corrected. For each combination of marker and RFP, images were thresholded and neuronal ROIs were counted as RFP and/or marker-positive and the resulting quantification for 2-3 DRGs per animal were averaged.

For enkephalin and NF200 double staining at dorsal spinal cord, slides were imaged using the Nanozoomer XR, whole slide scanning system at ×200 magnification with a resolution of 0.5 μm per pixel. WT and Nav1.7 KO sections were stained side-by-side on the same slides to avoid batch effects. Enkephalin expressing fibers were highly enriched in substantia gelatinosa of Rolando (SGR), which has a very low concentration of myelinated fibers and therefore is mostly NF200 negative. To examine Nav1.7 KO induced enkephalin up-regulation, SGRs (regions of interest, ROIs) were manually drawn on the dorsal horn of the spinal cord around lamina II, and the amount of staining in these ROIs was quantified in an automated fashion using integrated optical density. All image analyses were performed blind to genotype groups.

In situ hybridization

Dual ISH: Mm_Nav1.7-01 (red) / Mm_Penk-C2 (green)

The staining was performed on the Leica BondRX autostainer. RNAscope2.5 LS Duplex Assay kit (Advanced Cell Diagnostics cat#322440) was used for probe signal detection.

FFPE Tissue sections were cut @4um, loaded onto BondRX autostainer, bake and dewax, pretreatment sections with Bond ER2 (Leica Biosystems cat#AR9640) @88c for 15' and RNAscope® 2.5 LS Protease III @37c for5'.

Mm_Penk-C2 (Advanced Call Diagnostics Cat# 318761-C2, 50X) was diluted into Mm_Nav1.7-01(Advanced Cell Diagnostics Cat# 457648), dual probe hybridization for 120' @ 42°C. Modified RNAscope2.5 LS Duplex procedure resulted in Mm_Nav1.7-01 probe showing red signals and Mm_Penk-C2 probe showing green signals. Each AMP step incubation time followed ACD's recommendation. Mm_Nav1.7-01 chromogen color developed with mixed red refine reagent (Leica Biosystems Cat#DS9390) for 10'. Mm_Penk-C2 chromogen color developed with Permanent HRP Green Kit (Nordic Biosite cat#KDB-10049) for 5', Mayer's hematoxylin counterstain, tap water wash. Slides dry in 60c for 1h, cover slip.

Detailed AMP incubation steps and time

1. Bake and Dewax:
2. Pretreatment ER2 @88c for 15' ** RNAscope® 2.5 LS Protease III @37c for5'**
   - Dual probe hybridization: 120 MIN 42°C
   - RNAscope® 2.5 LS Duplex AMP 1 @30 MIN 42°C
   - RNAscope® 2.5 LS Duplex AMP 2 @15 MIN 42°C
   - RNAscope® 2.5 LS Duplex AMP 3 @30 MIN 42°C
   - RNAscope® 2.5 LS Duplex AMP 4 @15 MIN 42°C
   - RNAscope® 2.5 LS Duplex AMP 8 @15 MIN Ambient**
   - RNAscope® 2.5 LS Duplex AMP 6 @15 MIN Ambient
   - Mixed RED Refine Reagent @10 MIN Ambient

- RNAscope® 2.5 LS Duplex AMP 7 @15 MIN 42°C**
- RNAscope® 2.5 LS Duplex AMP 5 @15 MIN 42°C
- RNAscope® 2.5 LS Duplex AMP 9 @ 30 MIN Ambient
- RNAscope® 2.5 LS Duplex AMP 10 @15 MIN Ambient

Sequential Dual ISH_Mm_Penk(red) /IHC_TH(green) M&M

The staining was performed on the Leica BondRX autostainer. RNAscope2.5 LS Duplex Assay kit (Advanced Cell Diagnostics cat#322440) was used for ISH_Mm_Penk –C2 signal detection.

Part1: ISH_Mm_Penk

FFPE Tissue sections were cut @4um, loaded onto BondRX autostainer, bake and dewax, pretreatment sections with Bond ER2 (Leica Biosystems cat#AR9640) @95c for 15' and RNAscope® 2.5 LS Protease III @37c for5'. ISH_Mm_Penk -C2 (ACD cat# 318761-C2, 50X) diluted to 1X in RNAscope 2.5LS blank probe diluent (ACD cat#300048). Probe hybridization for 120' @42°C followed by RNAscope2.5 LS Duplex AMP1-AMP6 standard incubation time. Color developed with mixed red refine regent (Leica Biosystems Cat#DS9390) @10'.

Part2: IHC_TH

No additional antigen retrieval prior to IHC procedure. Polyclonal Rabbit anti tyrosine hydroxylase (Millipore cat#AB152)@1.6ug/ml for 60' followed by Powervision anti Rb-HRP (Leica Biosystems Cat# PV6119) for 30' and color developed with Permanent HRP Green Kit (Nordic Biosite cat#KDB-10049) for 5', Mayer's hematoxylin counterstain, Slides dry in 60c for 1h, cover slip.

Detailed AMP incubation steps and time

RNAScope2.5 LS Duplex Assay: only C2 channel signal was developed

1. Bake and Dewax:
2. Pretreatment ER2 @95c for 15' ** RNAscope® 2.5 LS Protease III @37c for5'*
   - Penk –C2 (50x) diluted to 1X in RNAscope 2.5 LS Blank Probe Diluent
   - probe hybridization: 120 MIN 42°C
   - RNAscope® 2.5 LS Duplex AMP 1 @30 MIN 42°C
   - RNAscope® 2.5 LS Duplex AMP 2 @15 MIN 42°C
   - RNAscope® 2.5 LS Duplex AMP 3 @30 MIN 42°C
   - RNAscope® 2.5 LS Duplex AMP 4 @15 MIN 42°C
   - RNAscope® 2.5 LS Duplex AMP 5 @15 MIN Ambient
   - RNAscope® 2.5 LS Duplex AMP 6 @15 MIN Ambient
   - Mixed RED Refine Reagent @10 MIN Ambient

Pain behavioral assays

All pain behavioral assays were performed by a blinded investigator unaware of the treatments or the genotypes of each animal. Groups of 6-12 animals were generally used for each test condition.

Randal Sellito

The threshold for mechanonociception was assessed using the Randall Selitto test. Mice were restrained in a soft cotton pocket held in the experimenter's hand. A 3 mm^2 blunt probe was applied to the middle of mouse tail with increasing pressure until the mouse exhibited a nocifensive response, such as tail withdrawal. The pressure required to elicit nocifensive behavior was averaged across three trials with inter-trial interval of 30 mins. The cut-off was 500g.

Hargreave's test

Spinal reflex responses to noxious heat stimulation were assessed using the Hargreaves' test.[45] Mice were habituated for an hour in plexiglass enclosures with a glass base. Before testing, the enclosures were cleaned of feces and urine. Radiant heat was then locally applied to the plantar surface of the hindpaw until the animal exhibited a nocifensive withdrawal response. Average latencies were obtained from three trials per animal, with inter-trial interval of 30 mins. Cut-off time was 30 s.

Acetone evaporation test

Animals are habituated for one hour in individual plexiglass test chambers on a wire mesh surface. A 1 ml syringe without a needle is filled with acetone and held tip upwards, and the plunger is pressed until a small amount of acetone emerges from the tip, held on by surface tension. This bubble of acetone is touched to the plantar surface of one hindpaw of each animal and the amount of time the animal spends reacting to this stimulus is recorded. The acetone begins to evaporate immediately upon contact with the animal's skin, producing a cooling sensation to which the animal typically reacts by shaking the affected hindpaw or holding it aloft, or licking the hindpaw or ankle. Acetone application will be repeated 3 times per animal, with inter-trial interval of 30 min.

Von Frey hair test

Punctate mechanical sensitivity was measured using the up-down method of Chaplan to obtain a 50% withdrawal threshold.[46] Mice were habituated for one hour in darkened enclosures with a wire mesh floor. A 0.4 g Von Frey filament was applied to the plantar surface of the paw for 3 s. A positive response resulted in application of a filament of lesser strength on the following trial, and no response in application of a stronger filament. To calculate the 50% withdrawal threshold, five responses surrounding the 50% threshold were obtained after the first change in response. The pattern of responses was used to calculate the 50% threshold = (10[c+kd])/10,000), where c is the log of the final von Frey filament used, k = tabular value for the pattern of responses and d the mean difference between filaments used in log units.

Hot plate test

Pain reflexes in response to a thermal stimulus (55°C) were measured using an IITC Model 39 Hot Plate Analgesia Meter. The mouse was placed on the hot plate within a transparent Plexiglas cylinder (15 cm D; 22.5 cm H) equipped with a Plexiglas lid and a timer is started immediately. A mirror is placed behind the hot plate so that the experimenter can observe the animal. The latency to respond with either a hind-paw lick or jump is measured to the nearest 0.1 s. The mouse is then immediately removed from the hot plate and returned to its home cage. If a mouse does not respond within 30 s, the test is terminated to avoid tissue damage. Average latencies were obtained from three trials per animal, with inter-trial interval of 30 mins.

Tail immersion test

Mice were restrained in a soft cotton pocket held in the experimenter's hand, so that the body is supported but the tail hangs outside freely of the pocket. Water in a standard water bath is warmed to 55°C. The distal one-third of tails were then immersed in the water. A timer is started immediately and latency to display a sharp flick of the tail out of the water is measured. and maximal cutoff latencies are set to 5 s. Average latencies were obtained from three to five trials, with 30 min inter-trail interval.

Cotton wisp test

The cotton wisp assay was performed as described previously.[47] Briefly, a wisp of cotton pulled up from, but still attached to a cotton swab was gently applied distal to the hawk region of the hind paw. Three applications were made to the hind paw with the interval of 15 min. A brisk withdrawal response was considered to indicate the presence of light touch evoked tactile allodynia.

Open field test for spontaneous locomotor function

Spontaneous locomotor activities were monitored by a 16 x 16 photobeam open field recording system and analyzed by an automated tracking program (PAS™, San Diego Instruments, San Diego, CA). One hour after oral administration of GNE-3565 (3, 10 or 30 mg/kg) or vehicle, mice were placed individually in transparent thermoplastic cages (40.5 (W) x 40.5 (L) x 38 (H) cm) and horizontal locomotor movements (ambulatory beam break, Amb BB) and vertical rearing movements were continuously recorded for one hour. The total number of beam breaks for both ambulatory locomotor activity and rearing were obtained for bin sizes of 10 min and reported as Amb BB and rearing per minute, respectively.

Blood pressure measurement with the CODA tail cuff method

Mouse peripheral blood pressures (BPs) were measured using the CODA non-invasive blood pressure system (CODA Monitor, Kent Scientific). Mice were put on a heating (37°C) pad and restrained in clear animal holders (HLD-MM-T) to which the mice had been previously conditioned. After 5-10 minutes acclimation, a volume pressure recording (VPR) cuff was attached to the tail distal to an occlusion cuff which occluded blood flow upon inflation. Systolic and diastolic BPs were then recorded during deflation and resume of blood flow. At least three to five separate blood pressure measurements were averaged from each animal.

Male and female mice were randomly divided into 3 groups: vehicle, 10 mg/kg and 30 mg/kg GNE-3565. Each group had 6 WT mice. After baseline BP measurements, the experimental animals were given vehicle or compound via oral gavage. One hour after administration, the BP of the same mouse was recoded again to compare the difference before and after the compound administration.

Laser speckle contrast imaging

Mice were anesthetized using sevoflurane in an appropriately sized induction box prior to and during laser speckle imaging. Once visually anesthetized, they will be transferred to a nose cone for anesthesia maintenance and put in a feedback-controlled heating pad for body temperature maintenance (37°C). To minimize breathing artifacts, mice were secured in ear bars. Ophthalmic ointment was applied to the eyes to prevent eye drying. Laser speckle contrast imaging (LSCI, moorFLPI-2, Moor Instruments, Wilmington, DE, USA) was used to monitor dermal blood flow (DBF) in the mouse hindpaws by assessing the flux in the imaging window over time.

A total 15 minutes LSCI movie was recorded for each animal at 5 Hz with 8.3 milliseconds exposure time, 0.3 seconds time constant and 5 x 5 pixels spatial kernel size for calculating the speckle contrast. The rectangular imaging window was cropped to include both hindpaws. After stable baseline recording (1 minute), 10 ul mineral oil (control) was applied to one hindpaw and 10 ul of 5% AITC was simultaneously applied to the other one. LSCI movie was continuously acquired during and after AITC skin challenge till the end of experiment.

Off-line Imaging analyses were performed using Moor Instruments analysis software. Regions of interest (ROIs) were drawn around the right and left hindpaws and the mean flux time-courses for each hindpaw were exported for further analysis in Matlab (verion 2016a, Mathworks). To remove breathing artifacts, the flux time-courses were low-pass filtered at 0.3 Hz using an equiripple filter and Matlab's filtfit function. Next, each time-course was normalized to baseline flux to calculate a fold change. The area under the curve (AUC) was calculated by integrating each fold change time-course from 2-6 minutes after imaging start to avoid the AITC application artifacts and to include the flux values up to the saturated responses at 6 minutes.

Properties and dosing of GNE-3565

GNE-3565 was identified during the course of drug discovery efforts targeting Nav1.7 and is described in the published patent US10457654B2 as example number 181.

GNE-3565 was dosed either p.o. or i.v.

For i.v. dosing, we used a formulation of 2 mg/ml GNE-3565 in 10% DMSO, 35% PEG400, 55% H_2O, pH=3 final with i.v. injection at 5 ml/kg over 10 min. Weigh about 10 mg of the compound in a 20 ml scintillation vial, add the DMSO (about 500 μl, sonicate/vortex/sonicate until fully dissolved (2 min is usually enough). Sometimes a tiny "hard" bit of compound is not dissolved. In this case, one should prolong the sonication/vortex/sonication cycle in DMSO until fully dissolved. Then add the PEG (about 1.75 ml), sonicate and vortex until fully dissolved. Add the water (about 2.75 ml), place a very tiny magnet in the vial, place on a magnetic stirrer, start stirring, plunge the pH probe (it just fits in) and add about 30-40 μl of HCl 1 N to reach pH=3 (first add 20 μl quickly, then the rest very slowly while watching at the pH value continuously). A 100 μl glass syringe fitted with fine tubing was used to deliver the HCl directly into the solution, not on the wall of the vial. The compound does not crash out of solution, even after a night in the fridge.

For p.o. dosing, GNE-3565 was suspended in 0.6% w/v Methylcellulose, 0.2% w/v Tween 80 in sterile filtered water (w/v %) by adding the vehicle to the powder, followed by mixing using vortex and sonication. Homogenization using Polytron was applied as necessary to generate a uniform suspension.

We have found that i.v. dosing achieves higher plasma concentrations of GNE-3565. At the highest oral dose tested (30mg/kg), we achieve an average total plasma concentration of 5.5μM (198nM free) at a Tmax of around 30min post dose as determined by mass spec measurements. Behavioral measurements are assessed at around 1 hour post dose, where the drug is coming back down a little bit, but it is still at around 3μM (108nM free). With i.v. dosing, we achieve around 10μM (360nM free) after the 10 min infusion at the highest dose we tested (10 mg/kg) or 2μM (108nM free) at the lower 3 mg/kg dose. Therefore, the level of compound in the plasma is about 3 times higher in the electrophysiology experiments at the highest doses tested. Thus, i.v. dosing provides a higher concentration of GNE-3565 and a more rapid increase in concentration after dosing relative to p.o. dosing.

An *in-vitro* biochemical assessment panel of potential off-targets of GNE-3565 was carried out at Eurofins. 10μM GNE-3565 was used in this assessment, which is more than 10x higher than the highest in-vivo free plasma concentration achieved in this study (360nM). The targets tested (all human) in this analysis were A1 (agonist radioligand), A2A (agonist radioligand), alpha 1A (antagonist radioligand), alpha 2A (antagonist radioligand), beta 1 (agonist radioligand), beta 2 (agonist radioligand), BZD (central) (agonist radioligand), D1 (antagonist radioligand), D2S (agonist radioligand), ETA (agonist radioligand), GABAA1 (alpha 1,beta 2,gamma 2) (agonist radioligand), GABAB(1b) (antagonist radioligand), kainate receptor (agonist radioligand), H1 (antagonist radioligand), H2 (antagonist radioligand), M1 (antagonist radioligand), M2 (antagonist radioligand), M3 (antagonist radioligand), nAChR neuronal alpha4beta2 (agonist radioligand), nAChR muscle-type (antagonist radioligand), kappa (KOP) (agonist radioligand), mu (MOP) (agonist radioligand), PPARalpha (agonist radioligand), PPARgamma (agonist radioligand), 5-HT1A (agonist radioligand), 5-HT1B (antagonist radioligand), 5-HT2A (agonist radioligand), 5-HT2B (agonist radioligand), 5-HT3 (antagonist radioligand), Ca2+ channel (L, dihydropyridine site) (antagonist radioligand), Ca2+ channel (L, verapamil site) (phenylalkylamine) (antagonist radioligand), Potassium Channel hERG [3H] Dofetilide, KV channel (antagonist radioligand), Na+ channel (site 2) (antagonist radioligand), Cl- channel (GABA-gated) (antagonist radioligand), norepinephrine transporter (antagonist radioligand), dopamine transporter (antagonist radioligand), 5-HT transporter (antagonist radioligand), PDE4D2 (enzyme activity assay), acetylcholinesterase (enzyme activity assay). We observed binding in the case of two targets: alpha 2A (85% displacement of yohimbine at 10μM GNE-3565), H1 (73% displacement of pyrilamine at 10μM GNE-3565), and 5-HT2B (54% displacement of DOI at 10μM GNE-3565). All other targets tested showed < 50% displacement of their respective radioligand at 10μM GNE-3565.

Synthesis of GNE-3565

Synthesis of 5-chloro-4-[[(1S,2S,4S)-2-(dimethylamino)-4-[3-(trifluoromethyl)phenyl]cyclohexyl]amino]-2-fluoro-N-pyrimidin-4-yl-benzenesulfonmnide

To methyltriphenylphosphonium bromide (14.2 g, 39.9 mmol) was added THF (44 mL). The suspension was cooled to 0°C and potassium tert-butoxide (4.47 g, 39.9 mmol) was added. The resulting yellow suspension was stirred at 0°C for 45 minutes. To the suspension was added a solution of **S1**, 1-(3-(trifluoromethyl)phenyl)ethanone (5.0 g, 26.6 mmol) in THF (22 mL) dropwise. The resulting mixture was then brought up to room temperature slowly and stirred for 16 hours. Reaction mixture was diluted with hexane (150 mL) and stirred for 20 min. The resulting precipitate was filtered, rinsed with hexane and the filtrate was concentrated. More hexane (200mL) was added to the residue and stirred for 20 min. The resulting precipitate was filtered through celite and the filtrate was concentrated to provide **S2**, 1-(prop-1-en-2-yl)-3-(trifluoromethyl)benzene (3.98 g, 80%) ^{1}H NMR (400 MHz, $CDCl_3$) δ 7.61-7.53 (m, 4H), 5.44 (s, 1H), 5.22-5.17 (m, 1H), 2.17 (dd, J=1.3, 0.7 Hz, 3H).

To iodine (33.9 g, 133.6 mmol) in DMA (180 mL) was added **S2** (4.98 g, 26.8 mmol) in DMA (5 mL). The reaction was stirred at room temperature for 20 minutes. A freshly made aqueous solution of saturated aqueous sodium thiosulfate was added as well as EtOAc (250 mL). The resulting solution was stirred for 10 minutes, water phase was removed and organic phase washed with water (2x50 mL) and with saturated aqueous brine solution (100 mL, then 50 mL) dried over $MgSO_4$, filtered and concentrated. The crude product was purified by flash column chromatography through Si gel (100% Hexanes) to provide **S3**, 1-(3-iodoprop-1-en-2-yl)-3-(trifluoromethyl)benzene (2.58 g, 31%). ^{1}H NMR (400 MHz, $CDCl_3$) δ 7.64 (d, J=8.3 Hz, 2H), 7.56 (d, J=8.2 Hz, 2H), 5.63 (s, 1H), 5.53 (s, 1H), 4.32 (s, 2H).

A solution of (S)-tert-butyl 4-ally1-6-oxo-1,3-oxazinane-3-carboxylate (2.0 g, 8.3 mmol) in THF (80 mL) was cooled to -78°C under nitrogen. KHMDS (0.5 M in Toluene) (16.6 mL, 8.3 mmol) was then added dropwise and the solution was left to stir at -78°C for 30 minutes. **S3**, 1-(3-iodoprop-1-en-2-yl)-3-(trifluoromethyl)benzene (2.07 g, 6.63 mmol) as a solution in THF (5 mL) was then added at once quickly and stirring was continued for 4.5 hours at -78°C. The reaction was quenched with saturated aqueous NH_4Cl solution (40 ml) at -78°C and then water (40 mL) and EtOAc (200 mL) were added. The organic layer was separated and washed with brine (2x40 mL) and then dried over Na_2SO_4 filtered and concentrated. The crude product was purified by flash column chromatography through Si gel (EtOAc/Hexanes) to provide **S4**, (4S,5S)-tert-butyl 4-allyl-6-oxo-5-(2-(3-(trifluoromethyl)phenyl)allyl)-1,3-oxazinane-3-carboxylate (1.29 g, 37%) as a clear oil. LCMS (ESI) m/z: 326.1 $[M\text{-}Boc+H]^+$.

S4, (4S,5S)-tert-butyl 4-allyl-6-oxo-5-(2-(3-(trifluoromethyl)phenyl)allyl)-1,3-oxazinane-3-carboxylate was dissolved in toluene (50 mL) and to this solution was added (Grubbs metal second generation (328mg, 0.39 mmol). The reaction mixture was stirred at 65°C for 6 hours. The reaction was cooled down to room temperature and purified directly by flash column chromatography through Si gel (EtOAc/Hexanes) to provide **S5**, (4aS,8aS)-tert-butyl 4-oxo-6-(3-(trifluoromethyl)phenyl)-2,4,4a,5,8,8a-hexahydro-lH-benzo[d][1,3]oxazine-l-carboxylate (926 mg, 90%). LCMS (ESI) m/z: 298.1 [M-Boc+H].

S5, (4aS,8aS)-tert-butyl 4-oxo-6-(3-(trifluoromethyl)phenyl)-2,4,4a,5,8,8a-hexahydro-lH-benzo[d][1,3]oxazine-l-carboxylate (920 mg, 2.32 mmol) was dissolved in THF (12 mL) and to the mixture was added a solution of lithium hydroxide (1.7 g, 69.4 mmol) in water (12.3 mL). The mixture was stirred at room temperature for 18 hours then acidified carefully with a 6M aqueous solution of HCl to pH∼3. The product was extracted by EtOAc (200 mL) and the organic layer was washed with saturated aqueous brine solution and dried over Na_2SO_4. The solvent was removed in vacuo to afford **S6**, (3S,4S)-4-((tert-butoxycarbonyl)amino)-3'-(trifluoromethyl)-2,3,4,5-tetrahydro-[1,1'-biphenyl]-3-carboxylic acid (845 m, 95%) and was used without further purification in the subsequent step. LCMS (ESI) m/z: 384.1 $[M\text{-}H]^-$.

To **S6**, (3S,4S)-4-((tert-butoxycarbonyl)amino)-3'-(trifluoromethyl)-2,3,4,5-tetrahydro-[1,1'-biphenyl]-3-carboxylic acid (845 mg, 2.19 mmol) in toluene (6.2 mL) was added triethylamine (0.43 mg, 3.06 mmol) and diphenylphosphoryl azide (0 52 mL, 2.41 mmol). The mixture was heated to 100°C for 35 minutes then cooled down to room temperature and purified directly by flash column chromatography through Si gel (EtOAc/Hexanes) to provide **S7**, tertbutyl((3S,4S)-3-(isocyanato-3'-(trifluoromethyl)-2,3,4,5-tetrahydro-[1,l'-biphenyl]-4-yl)carbamate (616 mg, 73%)

To **S7**, tertbutyl((3S,4S)-3-(isocyanato-3'-(trifluoromethyl)-2,3,4,5-tetrahydro-[1,l'-biphenyl]-4-yl)carbamate (615 mg. 1.60 nunol) in THF (3 mL) was added a solution of potassium trimethylsilanolate (248 mg. 1.93 mmol) in THF (1 mL). The mixture was stirred at room temperature for 18 hours then quenched by addition of saturated aqueous $NaHCO_3$ (20 ml) and the product was extracted with EtOAc (100 mL). The organic layer was separated, dried over

Na_2SO_4, filtered and concentrated to provide **S8**, tert-butyl((3S,4S)-3-amino-3'(trifluoromethyl)-2,3,4,5-tetrahydro-[1,1'-biphenyl]-4-yl)carbamate (507 mg, 88% yield) and was used without further purification in the subsequent step. LCMS (ESI) m/z: 357.1 $[M+H]^+$.

To **S8**, tert-butyl((3S,4S)-3-amino-3'(trifluoromethyl)-2,3,4,5-tetrahydro-[1,1'-biphenyl]-4-yl)carbamate (505 mg, 1.42 mmol) in methanol (4.7 mL) at 0°C was added formaldehedye (37% w/w in H_20) (1.06 mL, 14.2 mmol) followed by sodium cyanoborohydride (214 mg, 5.7 mmol). The reaction mixture was stirred for 1 hour at room temperature and then diluted with saturated aqueous $NaHCO_3$ (50 mL) and EtOAc (200 mL) and the phases were separated. The organic layer was washed with saturated aqueous brine solution, dried over Na_2SO_4 filtered and concentrated. The crude product was purified by flash column chromatography through Si gel (MeOH/DCM) to provide **S9**, tert-butyl((3S,4S)-3-(dimethylamino)-3'-(trifluoromethyl)-

2,3,4,5-tetrahydro-[1,1'-biphenyl]-4-yl)carbamate (422 mg, 77%). LCMS (ESI) m/z: 385.2 $[M+H]^+$.

To **S9**, tert-butyl((3S,4S)-3-(dimethylamino)-3'-(trifluoromethyl)-2,3,4,5-tetrahydro-[1,1'-biphenyl]-4-yl)carbamate (420 mg, 1.09 mmol) in ethyl acetate (5.5 mL) was added palladium hydroxide 20% on charcol (130 mg). The reaction was submitted to 3 cycles hydrogen/vacuum purged and then was stirred at room temperature for 4 hours under hydrogen atmosphere. The reaction was submitted to 3 cycles of nitrogen/vacuum purged, filtered through celite, rinsed with EtOAc and concentrated to provide **S10**, tert-butyl((1S,2S,4S)-2-(dimethylamino)-4-(3-(trifluorommethyl)phenyl)cyclohexyl)carbamate as a mixture of diastereoisomeres (323 mg, 77%). LCMS (ESI) m/z: 387.2 $[M+H]^+$. The mixture was used without further purification in the subsequent step.

To **S10**, tert-butyl((1S,2S,4S)-2-(dimethylamino)-4-(3-(trifluorommethyl)phenyl)cyclohexyl)carbamate (300 mg, 0.78 mmol) in DCM (2.6mL) was added 4 N HCl in dioxane (1 mL, 4 mmol). The reaction was stirred at room temperature for 2 h then concentrated and purified by C18 reverse phase flash chromatography (5-35% MeCN/10mM aqueous ammonium formate, pH=3.8). Appropriate fractions combined and lyophilized to provide **S11**, (1S,2S,5S)-N1,N1-dimethyl-5-(3-(trifluoromethyl)phenyl)cyclohexane-l,2-diamine (93 mg, 42%).

To **S11**, (1S,2S,5S)-N1,Nl-dimethyl-5-(3-(trifluoromethyl)phenyl)cyclohexane-l,2-diamine (100 mg, 0.35 mmol) in DMF (1.7 mL) were added DIPEA (0.19 mL, 1.05 mmol) and 5-chloro-N-(2,4-dimethoxybenzyl)-2,4-difluoro-N-(pyrimidin-4-yl)benzenesulfonamide

(239 mg, 0.52 mmol). The reaction mixture was stirred at 65°C for 18 hours and then quenched with water (10 mL). The product was extracted with EtOAc (50 mL), the organic layer was separated, washed with water, saturated aqueous brine solution dried over Na_2SO_4 filtered and concentrated. The crude product was purified by flash column chromatography through Si gel (0-20% MeOH/DCM) to provide **S12**, 5-chloro-N-(2,4-dimethoxybenzyl)-4-(((1S,2S,4S)-2-(dimethylamino)-4-(3-(trifluoromethyl)phenyl)cyclohexyl)amino)-2-fluoro-N-(pyrimidin-4-yl)benzenesulfonamide (250 mg, 99%). LCMS (ESI) m/z: 722.3, 724.3 $[M+H]^+$.

End product = 5-chloro-4-[[(1S,2S,4S)-2-(dimethylamino)-4-[3-(trifluoromethyl)phenyl]cyclohexyl]amino]-2-fluoro-N-pyrimidin-4-yl-benzenesulfonmnide

LCMS (ESI) m/z: 572.0 $[M+H]^+$. 1H NMR (400 MHz, DMSO-d_6) δ 8.37 (s, 1H), 8.15 (s, 1H), 8.03 (d, J=6.0 Hz, 1H). 7.68-7.60 (m, 3H), 7.58-7.55 (m, 2H), 6.75 (d, J=12.8 Hz, 1H), 6.66 (d, J=6.0 Hz, 1H), 5.88 (d, J=6.4 Hz, 1H), 3.65-3.63 (m, 1H), 3.20-3.15 (m, 1H), 2.85-2.80 (m, 1H). 2.39 (s, 3H). 2.39 (s, 3H), 2.16-2.11 (m, 1H), 2.10-2.01 (m, 1H), 1.78-1.73 (m, 2H), 1.69-1.58 (m, 1H), 1.41-1.37 (m, 1H).

QUANTIFICATION AND STATISTICAL ANALYSIS

Data quantification and statistical analysis was performed using GraphPad Prism (version 9.4). Tests were conducted in GraphPad Prism to verify the normality of the data. Statistical significance was assessed using paired or unpaired Student's t-test for comparison between two groups (WT vs. KO or control vs. drug treatment), Chi-squared for changes of TH^+ sensory neurons in WT and KO DRGs, one-way ANOVA or two-way ANOVA for comparison between multiple groups. The one-way and two-way ANOVA analyses were followed by post hoc comparison using Tukey's or Sidak's multiple comparison tests. Statistical tests used for specific experiments, the exact value of n, and what n represents in each analysis can be found in the corresponding figure legend. Data were presented as mean ± SEM and $p < 0.05$ was considered statistically significant.